

Dynamic planning and decarbonization pathways of the highway power supply network

En-jian Yao^a, Tian-yu Zhang^{a,*}, David Z.W. Wang^b, Jun-yi Zhang^c

^a Key Laboratory of Transport Industry of Big Data Application Technologies for Comprehensive Transport, Beijing Jiaotong University, Beijing, China

^b School of Civil and Environmental Engineering, Nanyang Technological University, 50 Nanyang Avenue, Singapore 639798, Singapore

^c School of Transportation, Southeast University, 2 Southeast University Road, Jiangning District, Nanjing 211189, China

ARTICLE INFO

Keywords:

Dynamic planning
Decarbonization pathway
Highway power supply network
Two-stage optimization model
Dynamic life-cycle assessment

ABSTRACT

This study attempts to explore dynamic planning and decarbonization pathways of the highway power supply network (HPSN) under four carbon emission reductions (CER) policies, including transport demand control, electrification of transport vehicles, transformation of regional power structure, and the highway energy self-sufficiency (HESS) construction. The developed dynamic deployment optimization and evaluation model includes three modules: (1) CER scenario quantification, (2) two-stage HPSN dynamic deployment optimization model, and (3) dynamic life-cycle assessment. Taking the HPSN of the Hoh-Bao-Eu-U urban agglomeration in China as a real case, 10 CER scenarios spanning from 2020 to 2050 are constructed. Firstly, the opportunities and challenges of the practical implementation of the HESS system are discussed. The HESS shows a strong potential role in the HPSN's decarbonization pathway. It could result in a 9.66 % reduction in peak carbon in 2035 and a 17.76 % increase in 2050 CER benefits compared to existing policies. Moreover, the multi-stage HESS project demonstrates positive economics, with the internal rate of return ranging from 12.14 % to 14.31 %. Further, the decarbonization pathways of the HPSN under various CER scenarios illustrate that the highway passenger car transport sector will achieve carbon peaking in 2030–2035, and the standardized carbon emissions in 2050 will range from 7.55 % to 56.56 % of those in 2020.

1. Introduction

Road transport carbon emission reduction (CER) is the key to achieving the Paris Climate Agreement goal of keeping the global average temperature rise within 2 °C and pursuing efforts not exceeding 1.5 °C. The historical process of CER in developed countries has shown that the share of greenhouse gas emissions from the transport sector in all sectors has continued to expand. Compared to 2022, CO₂ emissions from the transport sector in the US have increased by 1.49 % year-on-year [1] and become the top source of carbon emissions in the US [2]. In the same year, as a representative of developing countries, China's carbon emissions from the transport sector accounted for 11.1 % of global carbon emissions from the transport sector, following the United States at 21.3 % and the European Union at 11.2 % [2]. China's transport carbon emissions will predictably rise to the world's highest in the future, as the popularity of private cars and travel demand in developing countries is still in a rapidly rising phase. In China's transport sector,

road transport is the largest source of carbon emissions, accounting for up to 80 % in 2022 [3]. Therefore, the CER in the road transport sector will be a key part of achieving the carbon peak and carbon neutrality goals.

In recent years, rapid technological advancement and active policy support have brought new opportunities and strong confidence for the CER in the road transport sector. The public's purchasing willingness and trust in new energy vehicles (NEVs) has increased substantially with the increase in driving range, the improvement in charging speed, the decrease in the price of NEVs, and the continuous development of road charging networks [4]. In addition, the government has implemented a series of incentive measures for reducing carbon emissions in the highway passenger car transport (HPCT) sector, such as promoting NEVs, macro-regulation of vehicle ownership, and transforming the power supply structure. It is worth mentioning that China will take the lead in experimenting with constructing the highway energy self-sufficiency (HESS) system [5]. This system aims to achieve self-sufficiency in

* Corresponding author.

E-mail address: 21114038@bjtu.edu.cn (T.-y. Zhang).

electricity along highways through the collaborative deployment and operation of wind turbines (WT), photovoltaics (PV), energy storage (ES), and chargers.

A well-developed power supply network is a fundamental safeguard for the decarbonization of the road transport sector. Through the facilities deployment, planners can induce users' traveling and energy replenishment demand to achieve an efficient match between en-route charging loads and regional power supply. Existing research on planning networks of various types of energy supply facilities on highways is abundant. But there are still two limitations: a) In the planning process, planners mostly take the economics [6,7], the service level [8], and the safety [9] of the energy supply network as decision-making indicators while ignoring its CER benefits. This would result in the final deployment scheme that may not adequately respond to the government's CER goals. b) Studies on multi-stage planning of networks only consider the increase in electric vehicle (EV) penetration over time [10,12], ignoring changes in the external environment, such as power structure, equipment prices, etc. In addition, some economic and energy researchers have conducted in-depth analyses of decarbonization pathways under low-carbon goals at the national and sectoral levels [13–15]. However, the policy recommendations are more macro. It is urgent to research the decarbonization pathways for specific scenarios of each industry branch.

Therefore, this study attempts to explore dynamic planning and decarbonization pathways in the specific sector of HPCT. The specific questions addressed include: a) How should the highway power supply network (HPSN) be planned in an orderly sequence under various CER policies? b) How about the CER benefits and economic feasibility of the new initiative implementation of constructing the HESS system? c) How should different CER policies work together to help the HPCT sector meet the dual carbon goals?

Therefore, in response to the above issues, a dynamic deployment optimization and evaluation model for HPSN under the evolution of CER policies (DDOE-HPSN-CER) has been developed. Firstly, the social benefits on the HPCT sector of four categories of CER measures, namely, transport demand control (TDC), electrification of transport vehicles (ETV), transformation of regional power structure (TRPS), and HESS construction, are quantified at different periods. Subsequently, a two-stage HPSN dynamic deployment optimization model is designed for the HESS system involving multiple network couplings. It consists of Stage I: Bi-level dynamic deployment optimization of the charging network, and Stage II: Collaborative configuration of the HESS system. Finally, a dynamic life-cycle assessment (LCA) model is employed to assess the the long-term HESS project's return on investment (ROI) and environmental benefits. Additionally, this study conducts a case study on the highway network of the Hoh-Bao-Eu-U urban cluster in the Inner Mongolia Autonomous Region, China. 10 CER scenarios from 2020 to 2050 are constructed to simulate different CER degrees. Finally, the dynamic deployment schemes, energy-saving, emission reduction benefits, and ROI for HPSN under different scenarios are compared and analyzed.

Overall, this study is one of the few that explores the network planning and decarbonization pathways of HPSN under various CER policies. The contributions are summarized below:

- (1) In terms of methodology, the proposed DDOE-HPSN-CER model has the following targeted features. a) Macro-level CER policies are mapped to the meso-level facility planning model, enabling a quantitative analysis of the impact of CER policies on HPSN deployment and their environmental benefits. b) The proposed two-stage optimization model effectively decomposes the complex problem of collaborative operation and planning under multiple network couplings. c) The proposed dynamic LCA model thoroughly considers the changes in external factors over time, such as the CER policies, energy demand, energy structure, facility prices, and the corresponding dynamic deployment schemes.

- (2) At the same time, this study aims to provide more policy support for the decarbonization of the HPCT industry. a) The CRE benefits and economic feasibility of constructing the HESS system are highlighted. It provides significant guidance to the market on whether the HESS construction policy should be actively promoted in the future. b) The planning and decarbonization pathways of the HPSN under different CRE policy implementations during 2020–2050 are explored. It will provide policy support for decarbonizing the HPCT sector with sustainable services, positive environmental benefits, and good operational economics.

The remainder of this paper is arranged as follows. The related studies are reviewed in [Section 2](#). A conceptual model is described in [Section 3](#). The methodology is illustrated in [Section 4](#). Then, an empirical study is discussed in [Section 5](#). Last, the policy implications are concluded in [Section 6](#).

2. Literature review

2.1. Decarbonization pathways

In recent years, much literature in energy science, electric power, and the natural environment has been devoted to analyzing the future decarbonization pathways of various countries and industries. They focus on the energy system transformation under the low-carbon goal [13], the decarbonization pathway of each country [16,17,18], the impact of new energy generation equipment [14,19–20], and market policies on decarbonization [15], [21], and so on. Turning the spotlight on the transport sector, the researchers focus on the CRE potential of electric vehicles (EVs) [22–24]. They demonstrate the importance of growing EV penetration, smart charging strategies, and optimizing facility deployment to reduce energy consumption from the road transport sector while highlighting the concerns that high EV charging loads cause for grid security.

Most of the above studies focus on the macro level of energy and economy, and the policies and conclusions obtained from them are more suitable for guiding the decarbonization of the whole industry, the country, and even the world. The literature guiding the decarbonization pathway for the specific scenario of the HPCT has yet to be carried out. Exploring decarbonization pathways in the HPCT sector is urgently needed for governments to develop their medium- and long-term planning guidelines, for operators to invest in the energy supply infrastructure properly, and for people to plan their car purchases.

2.2. Planning of the highway charging network

In recent years, as the driving range of EVs increases and the process of transport integration in urban agglomerations continues to promote, the inter-city traveling demand of EV users has been rising. The planning scenarios for charging facilities have gradually shifted from the intra-city to the highway.

The framework of the highway charging network planning model is mostly the typical bi-level optimization [25–26]. Specifically, in order to capture the dynamic flow demand in the road network, flow capturing location-allocation models, e.g., static/dynamic traffic assignment, are mainly used as the lower model [11]. In the upper model, the location and capacity of charging facilities are optimized mainly from the perspective of construction investment economics [6–7], network service level [8], and grid security [9].

In addition, the highway charging network needs to dynamically adapt to the growing market's charging demands in the multi-stage process from zero EV percentage to full electrification [27]. The research on the multi-stage deployment problem is significant to the orderly construction and reasonable investment of the energy supply infrastructure. A few researchers have recently studied the multi-stage deployment problem of charging facility networks, transport

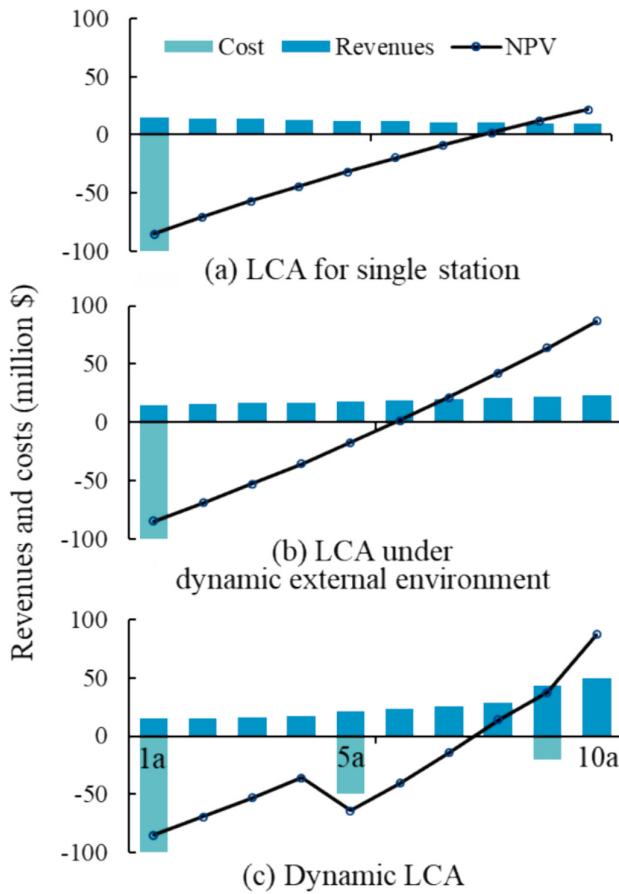


Fig. 1. The different LCA model for the project's economics.

networks, and power grids. Considering growing intercity trips, [28] proposed a multi-period multi-path refueling location model to optimize the extension of the charging network. [29] incorporated dynamic energy demand into multi-period capacitated flow refueling station planning considering the interaction of energy demand and the charging network. [10] developed multi-stage joint planning of charging stations and power grids for the growing number of electric buses.

The above research provides an essential foundational framework for this study's proposed multi-stage HPSN planning model. However, the current planning of the highway charging network has two limitations. First, the impact of the government's CER policies on the HPSN deployment path is not fully considered in its decision-making stage. It may lead the optimized deployment scheme to contradict the government's CER goals. Second, in the multi-stage HPSN planning model described above, the independent variable factors are only changes in EV penetration or vehicle ownership, which do not adequately consider the impact of external policies on users' travel, energy supply, and equipment prices. Therefore, conducting a study on the multi-stage planning pathway of the highway charging network in response to the CER policies is of great significance in guiding the government to formulate the medium- and long-term CER policy for the HPCT sector.

2.3. Economic and environmental assessment

A reliable cost-benefit and environmental benefit assessment of the power supply network is essential for the government's CER policy formulation and the operator's investment decision.

Based on the life-cycle theory, there has been some research on the comprehensive analysis of charging and battery swapping

infrastructures [30] [31], applied the life-cycle assessment to compare the life-cycle cost per bus kilometer between the wireless and plug-in bus systems. [32] analyzed the photovoltaic-energy storage charging station's economics and social benefits. Using the LCA tool, [33] discussed four types of chargers' energy consumption and greenhouse gas emissions and predicted their global warming potential changes during 2020–2040.

The studies mentioned above focused on assessing the cost-benefit and environmental benefit of various types of energy stations or static station layouts, and few studies assess the multi-stage network planning project. As an essential infrastructure in the highway decarbonization process, the HPSN will be planned with continuous construction for at least 30–50 years. Over such an extended period, investors and governments must accurately assess the economic and environmental benefits of the multi-stage HPSN deployment schemes under changing internal and external environments.

3. Problem description

In this section, the significance of HESS's collaborative planning and dynamic LCA is first explained and emphasized. Subsequently, a conceptual dynamic planning model for the HESS is presented, providing a brief overview of the entities involved, the objective function, and the constraints associated with the optimization problem. Finally, the challenges and application intractability of the proposed model are discussed, along with the suggestion of a model decomposition approach. This will aid in a rapid understanding of why the dynamic HESS planning problem is decomposed into two stages for resolution, providing a theoretical foundation for the model construction and solution in section 4.

3.1. The significance of the HESS's collaborative planning

In advancing vehicle electrification and energy-clean transformation, HESS appears to be one of the practical approaches for achieving carbon neutrality on highways. Ensuring the collaborative operation and planning among the various networks and equipment within the HESS will be crucial for realizing highway energy self-sufficiency.

The system is comprised of the transport network, the charging network, and the power generation network. Firstly, the topological structure of the transport network and the charging network jointly determine EV users' travel and charging behavior, thereby defining the spatial and temporal distribution of charging demand on highways. Furthermore, to ensure EV users' charging satisfaction, the charging network's service capacity needs to align with users' charging demands. Additionally, the equipment configuration of the power generation network must ensure the power supply and demand balance at the stations.

Therefore, the collaborative operation and planning of HESS will contribute to achieving the overall optimal performance of complex systems regarding economic efficiency, environmental benefits, and operational management.

3.2. The significance of the dynamic LCA

A well-developed HPSN is not established at once in the long-term decarbonization process on highways. Assessing the sustainability of the long-term dynamic HPSN project is a paramount concern for governments and businesses during the planning and investment phases.

Taking project economic evaluation as an example, Fig. 1 compares the assessment performance of different LCA methods. Fig. 1(a) illustrates the traditional LCA method. It only considers the one-time construction of facilities and overlooks changes in the external environment (such as demand fluctuations) and internal environment (such as facility expansions). At this point, influenced by the base discount rate, the

project's net present value (*NPV*) curve takes on a convex shape. This method is often employed for the LCA of individual new facilities. Building on the foundation of Fig. 1(a), LCA in Fig. 1(b) additionally considers the fluctuations in operating costs and revenues caused by changes in the external environment. Due to the omission of corresponding changes in the internal environment of the network, this LCA tends to overestimate the project's *NPV*. The proposed dynamic LCA is presented in Fig. 1(c). It simultaneously considers dynamic investments in facility expansion, as well as fluctuations in operating costs and revenues over long-term project planning and operation.

The dynamic LCA can comprehensively capture, analyze, and calculate changes in the project's internal and external environments at different stages. This enables a more precise estimation of the dynamic changes in economic, environmental, and managerial aspects during the project's long-term planning.

3.3. A conceptual dynamic deployment optimization model for the HPSN

In this study, the planning stages are represented by k with a total of k^* stages, where $k \in \{1, 2, \dots, k^*\}$. In stage k , the network topology of HPSN is abstracted as $N^k = (T, S^k, G^k)$. T represents the transport network, and its expansion or modification is not considered. The set of service area sites, denoted as ϕ , is selected as the candidate set of charging stations. S^k represents the charging network in stage k . It is composed of y_i^k , and CH_i^k . The binary variable y_i^k is the decision variable for charging network planning that $y_i^k = 1$ if a charging station will be built at site i in stage k , $y_i^k = 0$ otherwise. CH_i^k is the decision variable for the number of chargers at site i in stage k . G^k represents the power generation network, which is determined by the installed capacities of WT (PW_i^k), PV (PV_i^k), and ES (PE_i^k), and the installed output power of ES (E_i^k). Considering that petroleum fuel vehicle (PFV) users and hybrid electric vehicle (HEV) users do not have significant differences in travel and energy replenishment, the vehicle type $m \in \{fv, ev\}$ includes fuel vehicles (FV) and EV in the optimization phase. In the subsequent environmental benefit assessment, FV will be divided into PFV and HEV. T_1 is the period of traffic flow.

Next, a generalized dynamic deployment optimization model for the HPSN (DDO-HPSN) is formulated as follows.

(DDO-HPSN model)

$$\min_{\text{travelCost}}(\mathbf{v}(N^k), \mathbf{f}(N^k)) \quad (1)$$

$$\min_{\text{NPV-HESS}}(y_i^k, CH_i^k, PW_i^k, PV_i^k, PE_i^k, E_i^k, \Pi(N^k)) \quad (2)$$

s.t.

$$y_i^k \in \begin{cases} \{0, 1\} & \forall i \in \phi, k == 1 \\ \{1\} & \text{if } y_i^{k-1} == 0, \forall k \in \{2, \dots, k^*\} \\ \{0, 1\} & \text{if } y_i^{k-1} == 1, \forall k \in \{2, \dots, k^*\} \end{cases} \quad (3)$$

$$Q_i^k \in \left\{ \begin{array}{l} [0, y_i^k \cdot M] \\ [Q_i^{k-1} \cdot y_i^k, y_i^k \cdot M] \end{array} \right. \forall i \in \phi, k == 0 \quad \left. \begin{array}{l} \forall i \in \phi, k == 0 \\ \forall i \in \phi, k \in \{2, \dots, k^*\} \end{array} \right\} \quad (4)$$

$$T_i^{\text{avg}}(N^k) \leq T^{\text{avg}} \quad \forall i \in \phi, k \in K \quad (5)$$

$$T_i^{\text{max}}(N^k) \leq T^{\text{max}} \quad \forall i \in \phi, k \in K \quad (6)$$

$$L_{o,d}^m(T, S^k) = f_{\text{route}}(\cdot) \notin \emptyset \quad \forall o \in O, d \in D, m \in \{fv, ev\}, k \in K \quad (7)$$

$$P_x(T, S^k) = f_{\text{CHOICE}}(\cdot) \quad \forall x \in X, k \in K \quad (8)$$

$$WT_{x,i}(T, S^k), CT_{x,i}(T, S^k) = f_{\text{QUEUE}}(\cdot) \quad \forall x \in X, k \in K \quad (9)$$

$$\mathbf{v}(N^k), \mathbf{f}(N^k) = f_{\text{TRANS}}(\cdot) \quad \forall k \in K \quad (10)$$

$$\Pi(N^k) = f_{\text{POWER}}(\cdot) \quad \forall k \in K \quad (11)$$

where M is a sufficiently large integer. $T_i^{\text{avg}}(N^k)$ and $T_i^{\text{max}}(N^k)$ represent the average waiting time and maximum waiting time at site i under N^k . T^{avg} and T^{max} are the corresponding parameter thresholds. For the convenience of subsequent presentation, $x_{t,o,d,m,i}$ is abbreviated as x , denoting a type m user departing at time t from origin o to destination d via path l . And X is the set of x , $X = \sum_{t \in T_1} \sum_{o \in O} \sum_{d \in D} \sum_{m \in \{fv, ev\}} \sum_{l \in L_x(T, S^k)} x_{t,o,d,m,l}$.

$P_x(T, S^k)$ is the travel or charging choice of user x under (T, S^k) . $WT_{x,i}(T, S^k)$ and $CT_{x,i}(T, S^k)$ are the waiting time and charging time of user x at site i under (T, S^k) . $L_{o,d}^m(T, S^k)$ is the effective route set for the type m user departing from origin o to destination d . $\mathbf{v}(N^k)$, $\mathbf{f}(N^k)$, and $\Pi(N^k)$ are the traffic distribution matrix, charging decision matrix, and load matrix under the N^k .

In the dynamic planning of HPSN, it is necessary to ensure the interests of different entities at various stages. As shown in Eqs. (1)–(2), the objective function comprises two parts: minimizing the travel and charging costs for all users and maximizing the *NPV* for the HESS operator. Eqs. (3)–(4) together form the construction sequence constraints, representing constraints on locations and the capacities of various equipment in different stages. It is required that the stations already constructed in stage k be put into operation in stage $k + 1$, and the capacities of various equipment must be greater than or equal to the capacities in the previous stage. Eqs. (5)–(6) constraint the service level of each site in the HESS system. Eq. (7) represents the constraint on EV accessibility, requiring that the topological structure under the network (T, S^k) will meet the EV travel needs for each OD pair. Eqs. (8)–(11) together constitute the operational constraints of HPSN under the network N^k . They include constraints on user charging demand response $f_{\text{CHOICE}}(\cdot)$, station queue service $f_{\text{QUEUE}}(\cdot)$, traffic network flow transmission $f_{\text{TRANS}}(\cdot)$, and power transmission on the power generation network $f_{\text{POWER}}(\cdot)$.

3.4. Challenges and application intractability of the DDO-HPSN model

It is evident that the above model is a strongly NP-hard problem. The following two aspects mainly cause the difficulty in solving the model.

- (1) The computational catastrophe caused by the decision variables.

In the DDO-HPSN model, the decision variables include user decision variables $\mathbf{f}(N^k)$, network deployment variables y_i^k , CH_i^k , PW_i^k , PV_i^k , PE_i^k , E_i^k , and network operational variables $\mathbf{v}(N^k)$, $\Pi(N^k)$. Considering that the daily traffic flow on the highway reaches an order of magnitude of 10 million or more and the real-time calculation of various networks' status, it becomes challenging to solve it using exact optimization algorithms in operations research.

- (2) The limitations of traditional methods in estimating charging demand on highways.

The estimation of charging demand is the foundation of facility deployment optimization, and its accuracy directly influences the reliability of the layout scheme in future implementation. Many previous road network charging demand estimations have often employed a combination model of dynamic/static traffic assignment and Discrete/Continuous/Stationary queuing theory. However, such methods have certain limitations. On the one hand, traditional dynamic traffic assignment (DTA) treats users with the exact departure time and the same OD pair as a collective entity, overlooking the heterogeneity in users' travel and charging patterns. On the other hand, traditional mathematical queuing theory finds it challenging to

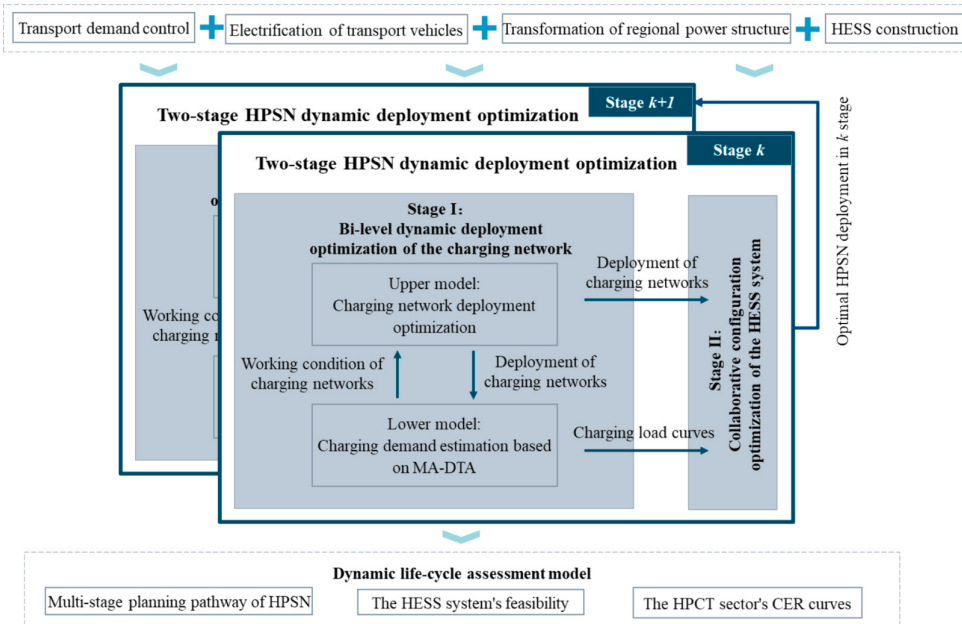


Fig. 2. The framework of the DDOE-HPSN-CER model.

accurately model the queuing and charging processes at sites for users who arrive randomly, discretely, and with varying charging requests.

In summary, the above DDOE-HPSN is decomposed into a two-stage model: Stage I: Bi-level dynamic deployment optimization of the charging network, and Stage II: Collaborative configuration optimization of the HESS system.

The decomposition approach is motivated by the interdependence among various networks, demand estimation accuracy, and optimization efficiency. Specifically, it includes the following aspects: 1) For EV users, charging decisions just consider the deployment and operational status of charging stations and chargers without concern for the source of power. 2) This study aims to construct an HPSN with a high service level. Therefore, EV users do not need to worry about issues related to insufficient power supply at charging stations. 3) For the second objective function in Eq. (2), the *NPV* of HPSN can be easily decomposed into the investment cost of the charging network and the *NPV* of the power generation network. They can be used as separate objective functions for the two-stage deployment optimization. 4) For the first-stage deployment optimization of the charging facility network, utilizing a bi-level optimization model to model the dynamic interaction between users and the charging network is highly reliable. 5) Employing multi-agent simulation methods to improve traditional DTA and queuing theory allows for precise estimation of the charging demands of EV users during highway travel.

4. Methods

To explore the HPSN's planning and decarbonization pathway, this study proposes a comprehensive model for the HPSN's deployment and assessment in multi-stage.

The framework of the DDOE-HPSN-CER model is depicted in Fig. 2. The notation of sets, parameters, and variables are listed in the Table A1. In the first step, based on the relevant historical data and planning goals, the impact of the currently implemented four CER policies on the HPSN planning in different stages is quantified. Further, the existing policy (EP) scenario, single policy scenarios, and multiple policies scenarios are developed to provide a basis for subsequent planning and assessment.

In the second step, based on the discussion in Section 3, the two-stage HPSN dynamic deployment optimization model is proposed. In Stage I, a dynamic deployment optimization of the charging network with a bi-level structure is developed. The high-precision heterogeneous enroute charging demand is captured based on the multi-agent-based DTA (MA-DTA) in the lower model. The charging station location and capacity are optimized in the upper model. Subsequently, in the second stage, an optimal configuration of each power generation equipment within HESS is performed. Based on the charging loads aggregated at the charging stations described above and the local average hourly wind and PV curves throughout the year, the power generation configuration that meets the sustainability of the power supply and the self-sufficiency of the energy use is solved.

In the last step, based on the life-cycle theory, the dynamic LCA is developed to evaluate the economic feasibility and CER benefits of HPSN from 2020 to 2050.

4.1. Scenario definitions

By reviewing the literature, government reports, and planning schemes, we summarize and generalize the CER policies involved in energy production from the energy side to energy consumption from the transport side in the HPCT sector. The relevant CER measures on the transport side can be divided into transport demand control and electrification of transport vehicles. The TDC policy attempts to reduce the amount of traveling by limiting the scale of the development of passenger cars. The ETV policy is the key to gradually switching the energy used by passenger cars from petroleum to power, thereby achieving zero carbon emissions from passenger cars on the traveling side. At the same time, on the energy generation side, the power will be further cleaned up through the TRPS and the HESS construction. Among them, under the TRPS policy, the power supply from the grid is cleaned up through the transformation of the region's overall energy structure. The HESS construction will achieve energy self-sufficiency in highway service areas through the coordinated operation and configuration of WT, PV, and ES.

Next, the various types of CER measures are described in detail. The implementation effects of different CER policies are quantitatively estimated for the years 2020, 2035, and 2050.

Table 1
Quantitative parameter settings under different scenarios.

Policies	Quantitative indicators	2020		2035		2050	
		EP	Deep	EP	Deep	EP	Deep
TDC	Passenger car ownership (million)	244	418	404	459	426	
ETV	EV penetration	1.75 %	22.5 %	24.3 %	50.1 %	75.8 %	
	HEV penetration	0.18 %	38.8 %	45.4 %	49.9 %	24.2 %	
TRPS	NFPG proportion %	33.90 %	38 %	55 %	53 %	77 %	
HESS	HESS construction	0	0	1	0	1	

- Transport demand control

Passenger car ownership in China has grown from 190 million units in 2015 to 319 million units in 2023. The continued high growth in passenger car ownership will bring considerable challenges to the country's transport and energy. For this reason, the government has issued a series of control policies towards transport demand, such as fuel tax increases, license plate lottery, carbon pricing setting, and transit-oriented development mode development. These TDC policies reduce passenger car ownership or travel at source.

[34,35] suggest that the thousand-passenger car ownership in China will reach 350 to 425 vehicles in 2050. Considering the traffic demand management measures such as driving restrictions, purchase restrictions, and public transport priority introduced in some Chinese cities, the EP scenario in this study sets the passenger car per 1000 people at 425 vehicles in 2050 and the domestic passenger car ownership at that time will be 459 million vehicles [36]. Passenger car ownership in China will decline further if travel structure optimization measures such as adjusting urban planning and encouraging green travel are taken. Therefore, under the deep TDC scenario, the number of passenger cars per 1000 people will be 350 in 2050, and the domestic passenger car ownership will be 426 million by then [36].

- Electrification of transport vehicles

Besides limiting the number of vehicles at the source, optimizing the energy structure of existing passenger vehicles is crucial. Governments encourage the public to purchase and use NEVs by implementing incentive policies such as price subsidies and parking priority. As a result, the energy structure of passenger cars is gradually shifting away from dependence on petroleum and towards cleaner power.

The development of NEVs is currently very powerful in China. The NEV sales in China account for 25.6 % of passenger car sales in 2022. Among them, EVs and HEVs are the dominant NEV types, accounting for 77.90 % and 22.04 %, respectively. Therefore, the ETV process in this study only considers the development trend of the above two types of NEVs, i.e., the penetrations of EVs and HEVs in different stages.

In the Energy Saving and New Energy Vehicle Technology Roadmap 2.0, the Chinese government calls for the penetration of NEVs in passenger vehicle sales to reach 50 % by 2035 and 100 % by 2060. Meanwhile, referring to the expanding trend of the current HEV market and related government policies, the penetration of EVs and HEVs under the EP scenario is set to reach 22.5 % (50.1 %) and 38.8 % (49.9 %) in 2035 (2050). Moreover, under the deep ETV scenario, with a 1.5 °C temperature control goal, the penetrations of EVs and HEVs are set at 24.3 % (75.8 %) and 45.4 % (24.2 %) in 2035 (2050) [2].

- Transformation of regional power structure

With the expansion of the NEV market scale, the level of power cleanliness (i.e., the proportion of non-fossil power generation (NFPG)) will directly impact the decarbonization process of the road transport

sector. In 2021, thermal power generation will remain the most dominant form of power generation in China, accounting for 69.77 % of the total. In response, the government requires upstream power generation to gradually transform the regional power structure. The proportion of green power will be increased by accelerating the construction of new energy infrastructure such as hydrogen stations, wind turbines, and photovoltaic panels and phasing out some coal-fired and gas-fired power plants early.

Under the EP scenario, according to the IEA's New Policy Scenario [37], it is assumed that China's NFPG proportion will increase to 38 % and 53 % by 2035 and 2050, respectively. Moreover, under the deep TRPS scenario, based on the IEA's Sustainable Development Scenario [37], the domestic NFPG proportion will rise to 55 % and 77 % by 2035 and 2050, respectively.

- HESS construction

The power system constructed in the service area of highways, where the operator needs to consider the volatility of natural resources and traffic load curves in time, will cause a huge security problem for the grid. At the same time, there are still serious technical bottlenecks in the grid integration of the surplus power in service area power systems [38]. Therefore, a grid-independent HESS system is proposed in China in 2021. The 14th Five-Year Renewable Energy Development Plan [39] states that it is required to actively promote the application of wind power and photovoltaic power generation in highway service areas and other transport areas.

This HESS construction guidance is still being discussed, and no specific policy guidance is available. Therefore, a deep HESS scenario is set up to explore the HESS program's feasibility. Under this scenario, the HESS system is constructed in an orderly to achieve self-consistency of power uses within the service area at all stages.

In summary, the expected indicators of the four CER policies for 2020, 2035, and 2050 under the EP and Deep scenarios are shown in Table 1.

4.2. Two-stage HPSN dynamic deployment optimization model

4.2.1. Stage I: Bi-level dynamic deployment optimization of the charging network

Based on the potential spatial and temporal distribution of en-route charging demands of EV users, operators need to deploy the charging network to determine the location and capacity of charging stations. In turn, the network deployment affects the route choice and EV users' energy replenishment choice behavior. A classic bi-level optimization model, with a charging network deployment optimization model in the upper layer and a charging demand estimation model in the lower layer, is developed to simulate this dynamic interaction.

- The upper model

Under the deployment scheme of the NPSN in stage k , the upper model optimizes the locations and capacities of charging stations for the next stage with the objective of minimizing the construction cost of the charging network. The upper model is formulated as follows.

(Stage I- upper model)

$$\min Z_1 = \sum_{i \in \phi} (y_i^k \cdot C_{\text{station}} + CH_i^k \cdot C_{\text{charger}}) \quad (12)$$

s.t.

Eqs. (3)–(7)

$$\mathbf{v}(N^k), \mathbf{f}(N^k) = \arg\min_{\mathbf{v}, \mathbf{f}} \sum_{x \in X} TC_x(T, S^k) \cdot q_{o,d}^{t,m} \cdot P_x(T, S^k) \forall k \in K \quad (13)$$

where C_{station} and C_{charger} are the fixed construction cost of unit charging

station and unit fast charger, respectively. $q_{o,d}^{t,m}$ is the loading flows for the type m user departing at time t from origin o to destination d .

The deployment scheme must satisfy the construction sequence constraints, service level constraints, and EV accessibility constraint as outlined in Eqs. (3)–(7). Furthermore, the interactive relationship of the bi-level model is formalized by Eq. (13), indicating that the charging demand originates from the lower model.

- The lower model

Considering the temporal volatilities of traffic flows, charging loads, road congestion, facility service levels, and users' traveling and charging heterogeneity, an MA-DTA model is developed as the lower model. To minimize users' travel and energy costs, a DTA model is applied to model the route choice and flow transmission of PFVs, HEVs, and EVs, and multi-agent-based simulation technology is used to simulate the service process of charging and queuing in the charging station. Ultimately, the individual heterogeneous charging demand and the daily working conditions of charging facilities are captured and transmitted to the upper model. The relevant mathematical formulas are shown as follows.

(Stage I- lower model)

$$\min Z_2 = \sum_{x \in X} TC_x(T, S^k) \cdot q_{o,d}^{t,m} \cdot P_x(T, S^k) \quad \forall k \in K \quad (14)$$

s.t.

Eqs. (8)–(10).

In Eq. (8), considering the heterogeneity of users, a path size logit model is employed to model the route and charging choices for FV and EV users. The specific formula is as Eqs. (15)–(17).

$$P_x(T, S^k) = \frac{\exp[-\theta \cdot TC_x(T, S^k) + \ln(M_{o,d,l})]}{\sum_{l \in L_x(T, S^k)} \exp[-\theta \cdot TC_x(T, S^k) + \ln(M_{o,d,l})]} \quad \forall x \in X, k \in K \quad (15)$$

$$TC_x(T, S^k) = \begin{cases} \sum_{a \in L_x(T, S^k)} \alpha \cdot \tau_{a,t} + \\ \sum_{i \in \phi} [\beta^{ev} \cdot H_{i,t}^{ev}(T, S^k) + (WT_{x,i}(T, S^k) + CT_{x,i}(T, S^k)) \cdot \alpha], m = ev \\ \sum_{a \in L_x(T, S^k)} (\alpha \cdot \tau_{a,t} + \beta^{fv} \cdot H_{x,a}^{fv}) m = fv \end{cases} \quad (16)$$

$$M_{o,d,l}^m = \sum_{a \in A_l} \left(\frac{\Delta l_a}{\Delta l_l} \cdot \frac{1}{\sum_{l \in L_{o,d}^m(T, S^k)} \partial_{a,l}} \right) \quad \forall m \in \{fv, ev\}, k \in K \quad (17)$$

where $H_{x,i}^{ev}(T, S^k)$ is the charging volume of vehicle x at site i . $H_{x,a}^{fv}(T, S^k)$ is the fuel consumption of vehicle x on road a . $\tau_{a,t}$ is the travel time of road a at t . Δl_a and Δl_l is the length of road a and route l . A_l is the road set of route l . $M_{o,d,l}$ is the correction term of route l from o to d . θ is the coefficient reflecting user perception differences. α is the time value. β^{ev} and β^{fv} are the prices of power and fuel.

Eq. (9) simulates the operation of the charging network. Its formalization is as follows.

$$WT_{x,i}(T, S^k) = \max \left\{ 0, \min_{b \in B_i(S^k)} \left\{ t_{c_i, b, t}^{CH}(S^k) \right\} - t_{x, c_i}^a(S^k) \right\} \quad (18)$$

$$CT_{x,i}(T, S^k) = 50 \ln[(s^{\text{exp}} - S_{x,i}(S^k)) / 0.9371 + 1] \quad (19)$$

where $B_i(S^k)$ is the set of chargers in site i . $t_{c_i, b, t}^{CH}(S^k)$ represents the remaining working time of charger b in site i at time t . $t_{x, i}^a(S^k)$ and $S_{x,i}(S^k)$ represents the moment and state of charge (SOC) when vehicle x arrives at site i under S^k , respectively. s^{exp} is the the expected SOC of the vehicle when leaving the charging station. Eq. (18) and Eq. (19) respectively calculate the waiting time and charging time for user x at site i under (T, S^k) .

In Eq. (10), the DTA with the point queue model is applied to model the dynamic flow transmission on the transport network. It mainly includes the node and link flow conservation constraints [25].

The MA-DTA model simulates the user's travel and charging responses and the charging station's operational process at a 15-min resolution. On the one hand, the modeling principle of the integration of operation and planning guarantees the operational sustainability of the charging network. On the other hand, the obtained charging load curves with high temporal resolution provide a reliable database for the subsequent Stage II.

4.2.2. Stage II: Collaborative configuration optimization of the HESS system

In stage II, the collaborative configuration of the HESS system is solved optimally. The model's inputs include the aggregated charging load curve of the station, the local yearly average curves of wind speed and solar radiation, and the performance of each type of equipment. To maximize the annual NPV of the power system, the HESS system's collaborative configuration optimization model optimizes the rated capacity and output power of the WT, the PV, and the ES.

There are four key principles behind the HESS system's collaborative configuration to ensure the power supply's reliability and economy: First, the conservation of power transmission: First, the conservation of power transmission. As the intermediary of the power transmission, the most basic requirement is to ensure that the power supply and dissipation in chargers and ESs are constant. Second, prioritize WT/PV power consumption and reduce or even avoid purchasing power from the grid. The power supply priority for charging stations is WTs/PVs, ESs, and grid in that order. Third, the system operates independently. The power generated by WTs/PVs is only consumed by local chargers and ESs to avoid the security impact of the distributed power generation on the local grid. Fourth, the equipment operates sustainably. It is necessary to impose reasonable constraints on the daily SOC of ESs to avoid the rapid decline of ESs' life caused by the deep discharge. The relevant mathematical formulas are detailed as follows.

(Stage II: HESS configuration optimization model)

$$\max Z_3 = NPV(PW_i^k, PW_i^k, PE_i^k, E_i^k, \Pi(N^k)) \quad (20)$$

s.t.

$$P_{i,t}^{D,k} = P_{i,t}^{R2C,k} + P_{i,t}^{E2C,k} \quad \forall i \in \phi, t \in T_2, k \in K \quad (21)$$

$$P_{i,t}^{E,k} = P_{i,t}^{R2E,k} - P_{i,t}^{E2C,k} \quad \forall i \in \phi, t \in T_2, k \in K \quad (22)$$

$$P_{i,t}^{R2C,k} = \min \left\{ P_{i,t}^{D,k}, P_{i,t}^{W,k} + P_{i,t}^{PV,k} \right\} \quad \forall i \in \phi, t \in T_2, k \in K \quad (23)$$

$$P_{i,t}^{D,k} = P_{i,t}^{W,k} + P_{i,t}^{PV,k} + P_{i,t}^{E2C,k} \quad \forall i \in \phi, t \in T_2, k \in K \quad (24)$$

$$P_{i,t}^{R2E,k} = \min \left\{ P_{i,t}^{W,k} + P_{i,t}^{PV,k} - P_{i,t}^{R2C,k}, \max \left\{ 0, \min \left\{ PE_i^k \cdot SOC_{\max}, PE_i^k \cdot SOC_{\min} \right\} \right\} \right\} \quad \forall i \in \phi, t \in T_2, k \in K \quad (25)$$

$$P_{i,t}^{E2C,k} = \min \left\{ \max \left\{ 0, P_{i,t}^{D,k} - (P_{i,t}^{W,k} + P_{i,t}^{PV,k}) \right\}, \min \left\{ PE_i^k \cdot SOC_{i,t}, PE_i^k \cdot SOC_{\min} \right\} \right\} \quad \forall i \in \phi, t \in T_2, k \in K \quad (26)$$

$$p_{i,t}^{PV} = PV_i^k \frac{G_{i,t}}{G_{\text{stc}}} [1 + \rho(T_{i,t} - T_{\text{stc}})] \quad \forall i \in \phi, t \in T_2, k \in K \quad (27)$$

$$p_{i,t}^{W,k} = \begin{cases} 0 & v'_{i,t} < v_{\text{in}} \text{ or } v'_{i,t} \geq v_{\text{out}} \\ PW_i^k \frac{v'_{i,t} - v_{\text{in}}}{v_{\text{rate}} - v_{\text{in}}} & v_{\text{in}} < v'_{i,t} \leq v_{\text{rate}} \\ PW_i^k v_{\text{rate}} & v'_{i,t} < v_{\text{out}} \end{cases} \quad \forall i \in \phi, t \in T_2, k \in K \quad (28)$$

$$SOC_{i,t+1}^k = SOC_{i,t}^k + \frac{\eta p_t^{E,k}}{PE_i^k} \Delta t \quad \forall i \in \phi, t \in T_2, k \in K \quad (29)$$

$$SOC_{i,t=0}^k = \delta \cdot PE_i^k \quad \forall i \in \phi, k \in K \quad (30)$$

$$SOC_{i,t=t^*}^k \geq SOC_{i,t=0}^k \quad \forall i \in \phi, k \in K \quad (31)$$

$$Q_i^k \in \left\{ \begin{array}{ll} [0, y_i^k \cdot M] & \forall k = 0 \\ [Q_i^{k-1} \cdot y_i^k, y_i^k \cdot M] & \forall k \in \{2, \dots, k^*\} \end{array} \right\} \quad \forall i \in \phi, Q \in \{PW, PV, PE\} \quad (32)$$

$$\lambda_{\min} E_i^k \leq PE_i^k \leq \lambda_{\max} E_i^k \quad \forall i \in \phi, k \in K \quad (33)$$

$$y_i^k, B_i^k = \underset{y_i, B_i}{\operatorname{argmin}} \sum_{i \in \phi} (y_i^k \cdot C_1 + CH_i^k \cdot C_2) \quad \forall i \in \phi, k \in K \quad (34)$$

$$p_{i,t}^{D,k} = \underset{v, f}{\operatorname{argmin}} \sum_{x \in X} TC_x(T, S^k) \cdot q_{o,d}^{t,m} P_x(T, S^k) \quad \forall i \in \phi, t \in T_1, k \in K \quad (35)$$

where $p_{i,t}^{D,k}$ is the load demand of site i at time t in stage k . $p_{i,t}^{W,k}$, $p_{i,t}^{PV,k}$, and $p_{i,t}^{E,k}$ are the output powers of WTs, PVs, and ESs at time t . $p_{i,t}^{R2C,k}$ and $p_{i,t}^{R2E,k}$ are the input powers from the Wind/PV generators to chargers and to the ES at time t . $p_{i,t}^{E2C,k}$ is the input powers from the ES to chargers at time t . $SOC_{i,t}^k$ is the real-time SOC of ESs in time t . SOC_{\min} and SOC_{\max} represent the upper and lower threshold values of ESs' SOC. $v'_{i,t}$ is the real-time wind speed. v_{in} , v_{out} , and v_{rate} are the cut-in wind speed, cut-out wind speed, and rated wind speed. $G_{i,t}$ and $T_{i,t}$ are the real-time solar irradiation and temperature. G_{stc} and T_{stc} are the solar irradiation and temperature under standard condition. η is the power efficiency. δ is the initial SOC of ESs during the day. T_2 is the period set of Stage II model. Δt is the time step. λ_{\min} and λ_{\max} are the lower and upper thresholds of the installed output power for ESs. ρ is the temperature coefficient.

Eq. (20) shows that the objective function is the maximum HESS system's annual NPV. The decision variables include the installed capacities of WTs, PVs, and ESs and the installed output power of ESs. Based on the above four key principles, the HESS configuration optimization model is constrained by Eqs. (21)–(35). Where Eqs. (21)–(26) is the conservation of power transmission. They modeled the power generation in WTs and PVs, power consumption in chargers, and power input and output in ESs. Eq. (24) requires that the power resources of chargers only be from the renewable power generators and the ES. It achieves energy self-sufficiency for the HESS system. The principle of power supply priority for chargers is formulated in Eqs. (25)–(26). Eqs. (27)–(28) represent the power generation models for WT and PV generators. Eq. (29) is the SOC update model for ESs. Then, the operation sustainability of ESs is constrained by Eqs. (30)–(31). It requires that the ES's SOC at the last hour during the day is not less than its initial SOC. Eqs. (32)–(33) shows the construction sequence constraints for various equipments. Last, shown as Eqs. (34)–(35), (T, S^k) and $p_{i,t}^{D,k}$ are originated from Stage I-upper model and Stage I-lower model, respectively.

4.3. Dynamic life-cycle-based assessment

In this section, the LCA model is developed to comprehensively assess the multi-stage HPSN planning pathway over the period 2020–2050 from the perspectives of energy and economics.

Over the system's life, the LCA model adequately considers time-varying factors, including the increase in vehicle ownership, changes in EV and HEV penetrations, infrastructure scale expansion, equipment degradation and updating, power structure transformation, inflation of money, and the decline in equipment prices. Last, CO₂ emission is used to assess the CER benefit of various scenarios. Moreover, the indicators, NPV, dynamic payback period (DPP), and internal rate of return (IRR), are used to assess the HPSN project's ROI.

4.3.1. Carbon emission calculation

Based on the multi-agent-based simulation platform, a "top-down" methodology is adopted to calculate the carbon emissions from en-route energy supplementation for all types of vehicles (PFVs, HEVs, EVs) on road trips. The annual carbon emission $E(N^k)$ for HPSN N^k is shown in Eq. (36).

$$E(N^k) = \sum_{m \in \{fv, gv\}} (D_m(N^k) \cdot EF_m / 100) + C(N^k) \cdot P_{fp} \cdot EF_{fp} \quad (36)$$

The first term $\sum_{m \in \{fv, gv\}} (D_m(N^k) \cdot EF_m / 100)$ calculates the annual carbon emissions of PFVs and HEVs under the scenario N^k . Where $D_m(N^k)$ denotes the annual mileage of PFVs and HEVs under scenario N^k . EF_m denotes the carbon emission factor per 100 km for PFVs and HEVs. For EVs, only the carbon emissions from thermal power are calculated, as the clean power sources are close to zero carbon emissions. $C(N^k)$ is the annual charging volume of EVs under scenario N^k . P_{fp} and EF_{fp} are the proportion of thermal power in the power structure under scenario N^k and its carbon emission factor, respectively.

4.3.2. Cost-benefit assessment

The ROI of the long-term HPSN project is the critical indicator that influences the investment incentives of service area operators. Therefore, the economic assessment of the multi-stage HPSN deployment is presented in this section. The time horizon for the whole HPSN project is 30a, and the superscript k is applied, where $k \in \{1, 2, \dots, 30\}$.

Based on the life-cycle theory, the costs and revenues of the multi-stage HPSN project in the manufacturing, use, and end-of-life stages are calculated in detail. In the manufacturing stage, the initial investment is made up of equipment purchase cost, distribution equipment cost, grid connection cost, and other cost, and construction subsidy income. In the use stage, the operation indicators of facilities and energy demand are the key to calculating the HESS system's annual costs and benefits. Based on the multi-agent-based simulation platform and the operation modeling for the HESS system, the annual power purchase cost, maintenance cost, operation cost, and power sales income are calculated. Last, in the end-of-life stage, equipment recycling income is also a source of revenue for operators. The relevant mathematical formulas are detailed in Appendix A. Next, the project's economic assessment indicators NPV, DPP, and IRR are described.

$$NPV = \sum_{k \in K} \frac{F^k}{(1+r)^k} \quad (37)$$

NPV calculates the difference between the total present value of revenues and expenditures in each stage of the project's life. Its formula is presented in Eq. (37). Where F^k is net cash flows in ka , $k \in K$; r is the base discount rate.

$$DPP = k^* - 1 + \frac{\sum_{k=0}^{k^*-1} F^k / (1+r)^k}{F^{k^*} / (1+r)^{k^*}} \quad (38)$$

The *DPP* is the period at which the project's cash inflows cover all expenditures, with consideration of money inflation. It is calculated in Eq. (38). Where k^* is the year in which the cumulative present value of net cash flows becomes positive.

$$NPV(IRR) = \sum_{k=0}^K \frac{F^k}{(1+IRR)^k} = 0 \quad (39)$$

The *IRR* is the rate of return when the program's cumulative yearly net cash flows are equal to zero over the period. It is calculated in Eq. (39). Generally, a project is regarded as feasible when its *IRR* is greater than or equal to the base rate of return.

4.4. Algorithm

The decomposed two-stage subproblems are solved by specialized optimization techniques tailored to each stage, potentially improving the overall efficiency of the optimization process. Below is the algorithm pseudocode.

Pseudocode of the proposed two-stage optimization model

Input: N , $q_{o,d}^{l,m}$, $v_{i,t}^l$, $G_{i,t}$ and $T_{i,t}$

```

1: Set the population size  $n^*$ , maximum iteration  $j^*$ , et al.
2: for  $k \in \{1, 2, \dots, k^*\}$  do
3:   Set  $j = 0$ 
4:   Buiding the initial population  $PO_{j=0}$  under Eqs. (3)-(4)
5:   while  $j \leq j^*$  do
6:     for  $n \in PO_j$  do
7:        $L_{o,d}^m(T, S^k) \leftarrow f_{\text{route}}(\cdot)$  //Depth First Search Algorithm
8:       if Eq. (7) satisfied do
9:          $Z_2 \leftarrow$ Eqs. (14)-(19) // MA & MSA
10:        if Eqs. (5)-(6) satisfied do
11:           $Z_1 \leftarrow$ Eq. (12)
12:        else
13:           $Z_1 \leftarrow M$ 
14:        end if
15:      else
16:         $Z_1 \leftarrow M$ 
17:      end if
18:    end for
19:    Update  $PO_j$  by selection/crossover/mutation under
       Eqs. (3)-(4),  $j \leftarrow j + 1$ 
20:  end while
21: Output:  $S^k$ ,  $v(N^k)$ ,  $f(N^k)$ ,  $p_{i,t}^{D,k}$ 
22: for  $i \in \phi$  do
23:    $Z_3 \leftarrow$ Eqs. (20)-(35) // Branch and Bound Algorithm
24: end for
25: Output:  $G^k$ ,  $\Pi(N^k)$ 
26: end for
```

Lines 3–20 present the algorithm for solving the bi-level optimization problem in Stage I. Due to the involvement of large-scale user decisions and dynamic inference of network states, a heuristic algorithm, namely the Genetic Algorithm, is employed as the main algorithm [25]. The multi-agent-based simulation technique is embedded into the Method of Successive Weighted Average to solve Stage I-lower model. The detailed pseudo-code for the corresponding algorithm has been provided in

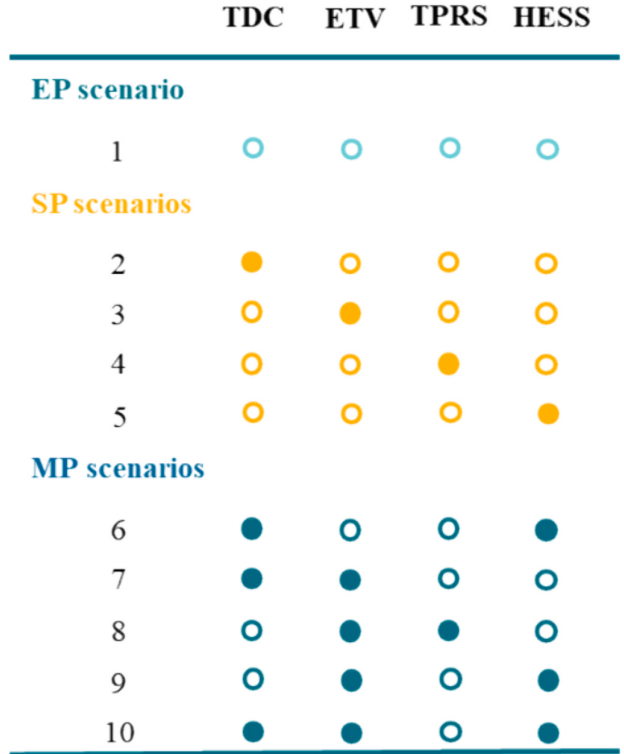


Fig. 3. The setting of 10 scenarios.

previous studies [40].

The solving process for the HESS configuration optimization problem is illustrated in lines 22–24. By employing linearization techniques, the min and max terms in Eqs. (23), (25), and (26) are linearly replaced, transforming Stage II model into a mixed-integer programming problem. Subsequently, the commercial solver Gurobi is utilized to perform an exact solution using the branch-and-bound algorithm. The process of model linearization is detailed in Appendix C.

5. Results

5.1. Case study input

This section explores the HPSN planning and decarbonization pathways for the Hoh-Bao-Eu-U urban agglomeration for 2020–2050 under different CRE policies.

The region is located at 41°N and spans from 109.89°E to 113.38°E. The landscape is vast and rich in wind photovoltaic resources. In the Inner Mongolia Autonomous Region, the “14th Five-Year Plan” on the comprehensive transport development plan [41] and renewable energy development plan [42] have pointed out that the service area along the highway should be reasonably distributed WT/PV power generation facilities, and create an innovative mode of the integration of traffic and energy.

Combining the above four CER policies, ten scenarios are designed, and the specific scenario information is presented in Fig. 3. Scenario 1 is the existing policy scenario that serves as the baseline. A single deep CER policy is imposed under scenarios 2–5. Under scenarios 6–10, multiple deep CER policies are imposed.

5.2. Long-term planning of HPSN

In this section, in an attempt to explore the multi-stage planning pathway of the HPSN and the construction feasibility of the HESS

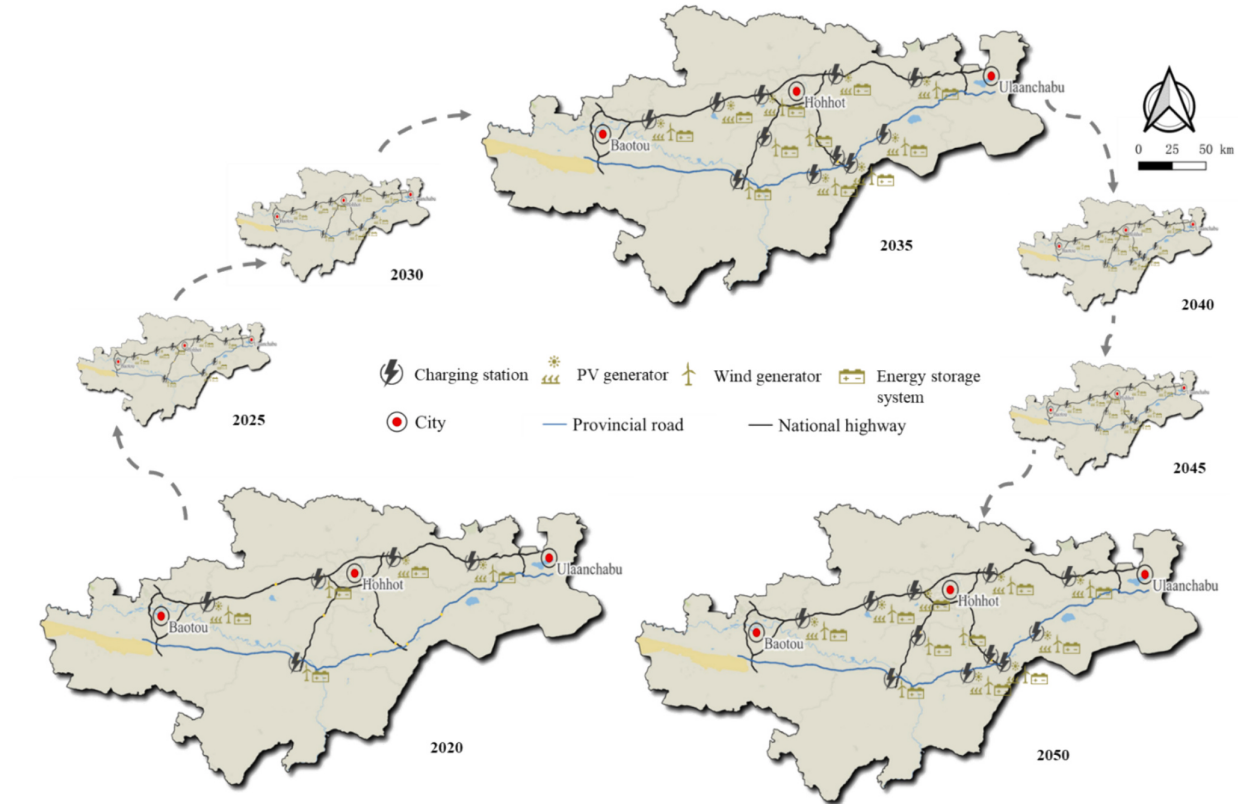


Fig. 4. The HPSN deployment schemes from 2020 to 2050.

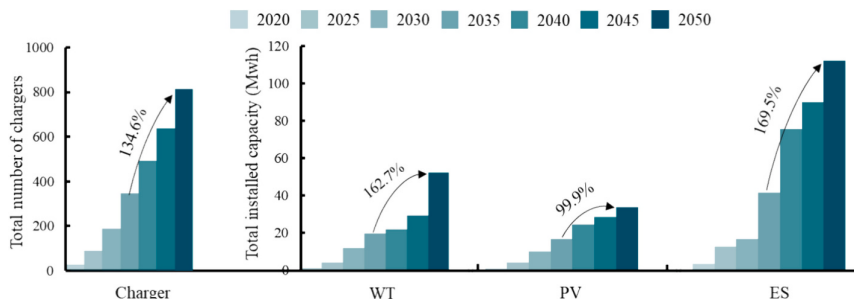


Fig. 5. The configuration of HPSN from 2020 to 2050.

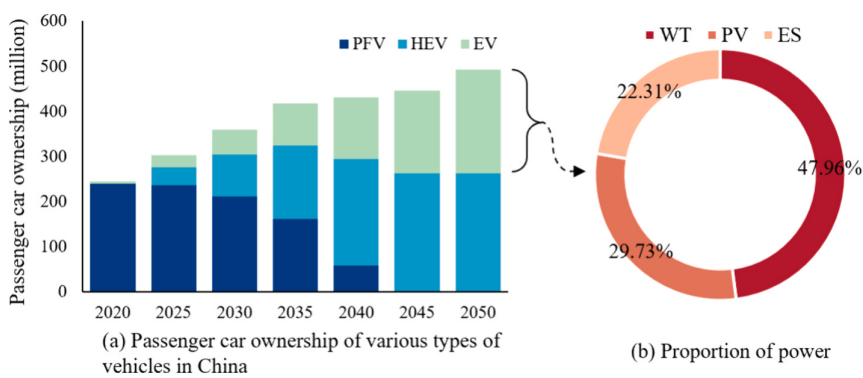


Fig. 6. The power supply of the HESS system from 2020 to 2050.

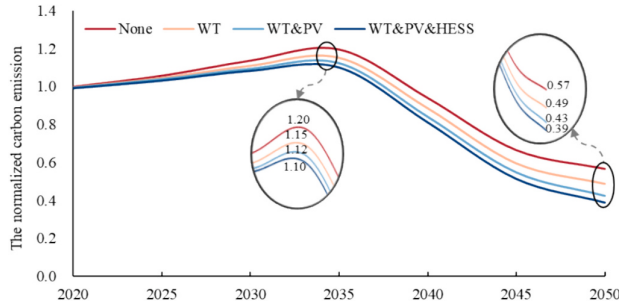


Fig. 7. The carbon emission curves with different power generation facilities from 2020 to 2050.

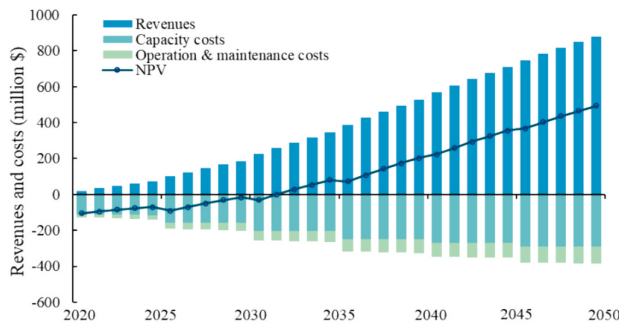


Fig. 8. The ROI of the HPSN project from 2020 to 2050.

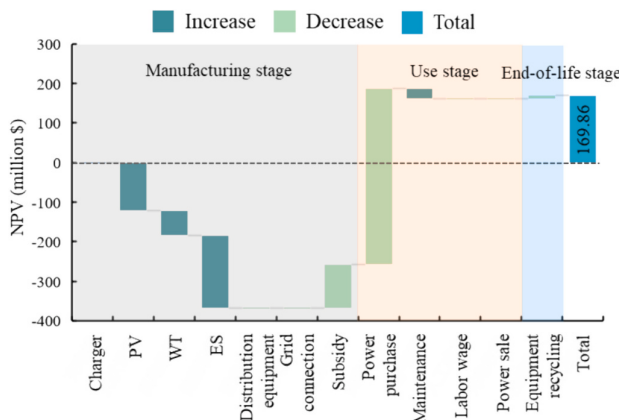


Fig. 9. The ROI comparison of the charging network and the HESS system.

system, Scenario 5 is taken as an example to specifically analyze its planning pathway, as well as its CRE benefits and ROI.

Fig. 4 shows the spatial pattern of the HPSN in each stage from 2020 to 2050. Among them, the deployment schemes for 2020, 2035, and 2050 are highlighted. By observing the locations of charging stations, it is found that the spatial pattern of the highway charging network continues to improve in the 2020–2035 period. During this period, charging stations are prioritized for being built on highways with higher road levels and greater travel demand than provincial roads. And the highway charging network will achieve its final spatial layout in 2035, i.e., no more new charging stations will be built. In addition, as complementary power generation facilities, WT and PV do not need to be constructed simultaneously at all stations. The most economical power generation facility should be installed according to the local natural resources. As an intermediary for storing and discharging power, the ES

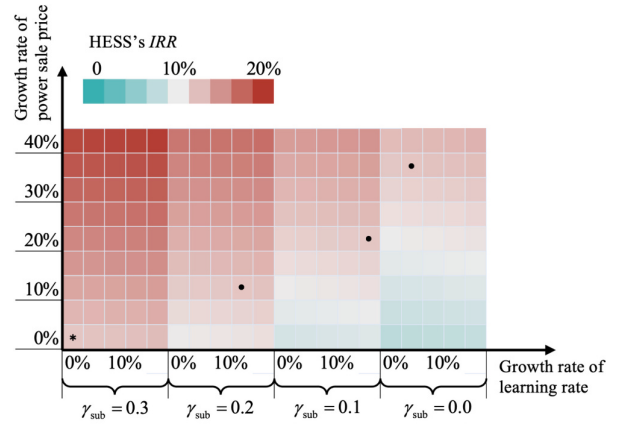


Fig. 10. The IRR of the HESS system in various scenarios.

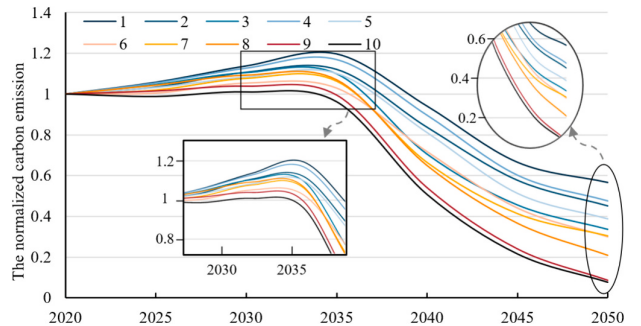


Fig. 11. The normalized carbon emission curves over the period 2020–2050 under each scenario.

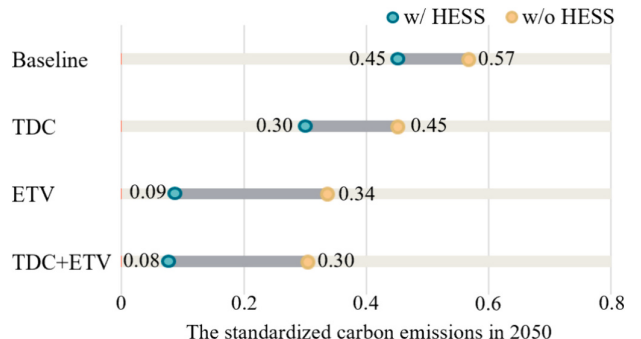


Fig. 12. The comparison of 2050 CER benefits under different scenarios.

is an indispensable device for the HESS system to realize the function of energy self-sufficiency.

Fig. 5 statistically details the configuration of the various facilities within the HESS system over six stages. From 2035 to 2050, HPSN's service and generation capacities will substantially increase to meet the rapidly increasing demand for EV charging. The average number of chargers at a station grows from 31.5 to 74.0. Meanwhile, for power generation, the installed capacities of WT, PV, and ES rise by 162.7 %, 99.9 %, and 169.5 %, respectively. The deep transformation of vehicle electrification in the mid to late stage (2035–2050) will significantly challenge HPSN's operation and management.

Further, the power supply of the HESS system in different stages is discussed. Fig. 6(a) shows the travel intensity of various vehicles on the

Table 2

The ROI of HESS projects with other different policy combinations.

	NPV (million \$)	DPP	IRR
Baseline+HESS	495.08	11.99	12.14 %
TDC + HESS	486.98	9.78	13.38 %
ETV + HESS	655.44	11.21	13.56 %
TDC + ETV + HESS	634.34	9.80	14.31 %

Table A1

The abbreviation.

CER	Carbon emission reduction
NEV	New energy vehicle
HPCT	Highway passenger car transport
HESS	Highway energy self-sufficiency
WT	Wind turbines
PV	Photovoltaics
ES	Energy storage
HPSN	Highway power supply network
DDOE-HPSN-CER	Dynamic deployment optimization and evaluation model for HPSN under the evolution of CER policies
TDC	Transport demand control
ETV	Electrification of transport vehicle
TRPS	Transformation of regional power structure
LCA	Life-cycle assessment
ROI	Return on investment
EV	Electric vehicle
PFV	Petroleum fuel vehicle
FV	Fuel vehicle
DDO-HPSN	Dynamic deployment optimization model for the HPSN
EP	Existing policy
DTA	Dynamic traffic assignment
MA-DTA	Multi-agent-based dynamic traffic assignment
HEV	Hybrid electric vehicle
NFPG	Non-fossil power generation
SOC	State of charge
NPV	Net present value
DPP	Dynamic payback period
IRR	Internal rate of return

highway. The travel demand on highways will continue to increase from 2020 to 2050. With the implementation of the no-fuel policy in 2030, all PFVs will be replaced by HEVs and EVs in 2045. Furthermore, the EV travel proportion will be over 50 % for the first time in 2050. Further, the breakdown of the power sources for EVs is shown in Fig. 6(b). Within the HESS system, the power supply of the chargers comes from WT, PV, and ES. Among them, WT generates the largest amount of power, averaging 47.96 % of the total power in 2020–2050. It is followed by PV and ES, which supply 29.73 % and 22.31 % of the total power in 2020–2050, respectively.

To further analyze the CER benefits of various types of power generation facilities, the carbon emission curves of the HPCT sector with different power generation facility configurations from 2020 to 2050 are compared. To make the a more generalized discussion, the CER curves are normalized based on the network carbon emissions in 2020 as the baseline value. Fig. 7 depicts the normalized carbon emission curves under the configuration of charging station only, charging station & WT, charging station & WT & PV, and HESS system. Compared to the charging network, the carbon peak time of the HPCT sector under the

Table B2

The other parameters.

P_{dis}	357.2 \$	δ_{ch}	22 kW
ν_{ch}	0.7	α_{cs}	0.85
L_{\max}	0.8	$\cos\phi_{\text{ch}}$	0.95
η_{ch}	0.9	P_{buy}	1\$/kWh
$P_{\text{land},i}$	3 million \$	$\gamma_{\text{ma,a}}$	0.04
$\gamma_{\text{ma,c}}$	0.03	N_{lab}	9
P_{lab}	52,486 \$	l_{WT}	20
l_{charger}	10	l_{ES}	15
l_{PV}	30	γ_{sub}	30 %
P_{ser}	0.5\$/kWh	γ_{sal}	5 %

P_{dis} , ν_{ch} , δ_{ch} , L_{\max} , α_{cs} , η_{ch} , and $\cos\phi_{\text{ch}}$ are from [27]. $\gamma_{\text{ma,c}}$, $\gamma_{\text{ma,a}}$, and γ_{sal} are from [44]. γ_{sub} is from [32]. P_{buy} , P_{buy} , P_{ser} , and P_{lab} are set up according to the real situation in China.

HESS construction is still 2035, but its peak value decreases by 9.66 %. And the network's CRE benefit in 2050 (compared to 2020) is enhanced from 43.4 % (1–56.6 %) to 61.2 % (1–38.8 %). In further analysis, the CER benefits of WT, PV, and ES for the HPCT sector are sequentially lower. Their benefits of CRE enhancement in 2050 are 7.69 %, 6.36 %, and 3.71 %, respectively.

Fig. 8 shows the ROI of the HPSN project over the 2020–2050 period. In the preliminary stage of HPSN development, operators and governments have to bear a heavy financial burden due to high infrastructure investment costs and low facility utilization rates. The DPP of the project is 11.99 years, which means that the HPSN operator will break even for the first time in 2032. As the infrastructure improves and the EV market expands, the HPSN project is gradually becoming profitable, with an NPV of \$495 million by 2050. Overall, the HPSN project has an IRR of 12.14 % over the 2020–2050. This value is at the industry average (10 %–20 %), implying that this project has a good investment prospect.

Next, the ROI of the only charging network and the HESS system are compared, as shown in Fig. 9. The change in the ROI of the HESS system compared to the charging network is driven by three main factors: the savings in power generation revenues from not relying on grid purchases, the investment cost in WT, PV, and ES equipment, and relevant government construction subsidies. In the manufacturing stage, the construction of power generation equipment imposes a large financial burden on the operator and the government. This ultimately leads to a lower IRR of 4.5 % for the HESS system project compared to the charging network project. However, in the use stage, the savings in purchased power costs ultimately result in a 52.3 % higher NPV in 2050 for the HESS system project compared to the charging network project (\$495 compared with \$325 million). This suggests that the HESS project has a better ROI but is built on a greater infusion of investment capital.

Further, the impacts of HESS equipment's technology development speeds and power price growth ratios on the project's IRR after reduced construction subsidy policies are analyzed. Based on the parameter settings of the base scenario, the construction subsidy coefficient is set at four levels: 30 %, 20 %, 10 %, and 0 %. The growth rate of learning rate for each type of equipment is set at 0 %–20 % with an interval of 5 %. The growth rate of the power sales price is set at 0 %–40 % with an interval of 5 %. Fig. 10 displays the project's IRR under different

Table B1

The dynamic equipment price.

	Learning rate	2020	2025	2030	2035	2040	2045	2050
P_{charger}^k	18 %	42	20.2	16.2	14.8	14.2	13.6	13.1
P_{WT}^k	11.78 %	3.5	3.0	2.8	2.6	2.5	2.4	2.3
P_{PV}^k	32.4 %	12.6	6.9	3.1	2.9	2.6	2.5	2.3
P_{ES}^k	18 %	4.3	3.5	2.7	2.6	2.4	2.2	2.0

The learning rate and the price in 2020 of each equipment are from [14]. The dynamic equipment price during 2025–2050 is predicted by the learning rate and the number/volume of each equipment in the future. The initial capacity of each equipment in 2020 is from [43]. Note: the unit of price is \$1000, and \$ is RMB.

scenarios, denoted as (construction subsidy rate, growth rate of learning rate, and growth rate of power sales price). In this case, the square marked with a star is the base scenario (30 %, 0 %, 0 %), and squares marked with black dots are scenarios with an IRR close to the base scenario's IRR.

The analysis reveals that: 1) The construction subsidy significantly impacts the HESS's IRR. With the learning rate and power sales price unchanged, the systems' IRR decreases to 8.66 % and 7.32 % when the subsidy rate is 10 % and 0 %, respectively. This indicates that HESS projects have a poor ROI and are unsuitable for investment in these situations. 2) The impact of reduced construction subsidies on the HESS economics can be effectively compensated by equipment technology development and power sales price growth. In particular, the IRR of the combined scenarios (20 %, 15 %, 10 %), (10 %, 20 %, 20 %), (0 %, 5 %, 35 %) is close to the 12.14 % of the baseline scenario. 3) The IRR enhancement for HESS projects is more significant for power sales price growth compared to the equipment's learning rate growth. Compared to the baseline scenario, the IRR in the (30 %, 20 %, 0 %) and (30 %, 0 %, 20 %) scenarios improves by 0.51 % and 3.51 %, respectively. This value is further improved to 4.00 % in (30 %, 20 %, 20 %) scenario when both are increased.

5.3. Long-term plannings in various policies

This section conducts a comparative study of the decarbonization pathways in the HPCT sector under scenarios 1–10.

First, the following two terms related to CER benefits are introduced for the convenience of the subsequent discussion. Peak carbon-cutting benefit: the normalized carbon peak reduction rate under different scenarios compared to that of the baseline scenario. 2050 CER benefit: the normalized CER reduction rate under different scenarios compared to that of the baseline scenario in 2050.

The normalized carbon emission curves over the period 2020–2050 for each scenario are plotted in Fig. 11, based on the total carbon emissions in 2020 as the baseline value.

The carbon emissions pathways in the HPCT sector show a three-stage trend of slow increase followed by rapid decline and then slow decline. Under different scenarios, the HPCT sector's carbon emissions will peak during 2030–2035, which is 1.0 % to 19.6 % higher than the emission level in 2020. There is no significant change in the carbon peaking time with the implementation of a single deep TDC, TRPS, and HESS policy, and their Peak carbon-cutting benefits are 2.19 % to 9.66 %. The HESS construction is the most effective single policy for cutting the carbon peak. Under the deep ETV scenario, the carbon peaking time would be advanced from 2035 to 2030, and its Peak carbon-cutting benefit is 9.21 %. The Peak carbon-cutting benefits of the network will be further enhanced to 10.4 %–18.6 % with the combined support of multi-deep CER policies. Their carbon peak times in the HPCT sector will both be reached around 2030. In particular, the growing trend of carbon emissions in the HPCT sector can be well controlled by the combination of deep ETV, TDC, and HESS policies. Its carbon emissions remain largely constant over the 2020–2035 period.

There is a large variability in the HPCT sector's carbon emissions in 2050 under different scenarios, with standardized carbon emissions ranging from 7.55 % to 56.56 % of those in 2020. In implementing the single deep CER policy, the 2050 CER benefits of ETV, HESS, TRPS, and TDC decreased in order, with 22.99 %, 17.76 %, 11.39 %, and 9.07 %, respectively. Further, the 2050 CER benefits of the network are improved with the collaborative effect of multiple measures. It is worth noting that the HPCT sector's carbon emissions in 2050 will be less than 10 % of that of 2020 under Scenario 9 and Scenario 10. This would be expected to achieve carbon neutrality in the HPCT sector.

Next, the collaborative effects of the HESS policy with other policies are explored. The CER benefits and ROI of HESS construction under other different policy combinations are compared, as shown in Fig. 12 and Table 2. Fig. 12 shows that the HESS construction can enhance the

2050 CER benefits in the HPCT sector by 15.21 % to 25.00 %. Among the combinations with other policies, the collaborative benefit of HESS with ETV policy is the largest. The construction of HESS can improve the 2050 CER benefits by 25.00 % and eventually reach 8.57 %, based on the implementation of the ETV policy. As shown in Table 2, the DPP of the HESS system is between 9 and 12 years, and its IRR is between 12.14 % and 14.31 % under different scenarios, which indicates that this HESS system has good investment economics under various CER scenarios.

6. Policy implications and conclusions

The spatial structure of the highway charging network is expected to be largely complete by 2035, which will be able to cover the en-route charging demands of the entire network. The focus of the HPSN planning shifts from expanding the charging service coverage in the early period (2020–2035) to improving the node charging service capacity and power generation capacity in the later period (2035–2050). Therefore, when selecting charging station locations in the early stage, it is necessary to give special consideration to the field space, capital investment, and operation and management pressure required for the infrastructure expansion in the later stage.

This study focuses on the CER benefits and ROI of the new initiative of constructing the HESS system. Opportunities and challenges in the practical implementation of the HESS system are analyzed.

In the HPCT decarbonization process, the development of HESS is critical to achieving the dual-carbon goals by 2050. The HESS construction is the single policy with the most significant peak carbon reduction and the second-largest 2050 CER benefit. Its Peak carbon-cutting benefit is 9.66 %, and its 2050 CER benefit is 17.76 %. In conjunction with a different policy mix, the construction of the HESS system will result in a further 15.21 %–25.00 % reduction in carbon emissions by 2050 in the HPCT sector. It is important to note that the key to fully exploiting the CER benefits of the HESS system is the collaborative management of multiple energy sources as well as the coordinated operation and configuration of natural resource-based generation equipment and ESs. The collaborative management of multiple energy sources can effectively complement the power generation of natural resources such as wind and photovoltaic, which have fluctuating and intermittent properties in the temporal and spatial dimensions. In Case 5, the inclusion of PV leads to a 6.36 % increase in the 2050 CER benefit compared to the single WT. In addition, the coordinated operation and configuration of natural resource-based generation equipment and ESs enhances the efficiency of HESS by absorbing and releasing natural resource power through ESs. In Case 5, ES is built at each station, and its application increases the CRE efficiency by 3.71 % in 2050.

In terms of economics, the HESS project has demonstrated a positive ROI. Its IRR will maintain 12.14 % to 14.31 %, and DPP is about 9 to 12 years under various planning pathways. NPV of HESS projects increased by 52.3 % compared to single charging station projects. This will strengthen the confidence of governments and operators in promoting the construction of HESS. However, there are certain investment risks associated with the HESS project. The current high construction subsidy rate is the key to promoting the HESS project in the early stages. With the expansion of the HESS construction scale, the government will face substantial financial pressure. The analysis found that once the subsidy rate is reduced to 10 % or even canceled, the IRR of HESS projects will drop to 8.66 % or even 7.32 %. This will make HESS projects less economically attractive. To achieve sustainable development of the HESS project, government subsidies should be reduced orderly without affecting the ROI of the project. On the one hand, the negative impact of reduced subsidies on the HESS project's ROI could be compensated by the advancement of equipment technology and the adjustment of power sale prices. Accelerating the technological development of generation equipment and ESs will decrease the investment cost of HESS. The increase in power sale price significantly improves the IRR of HESS projects. However, unquestioningly increasing the price is not conducive to

developing the NEV market. Attempts can be made to increase users' willingness to spend during charging dwell time through value-added services, such as increasing service businesses or service levels in the service area. In addition, the government should actively develop new types of Public-Private Partnership operation modes, such as Build-Operate-Transfer, Build-Operate-Own, and Transfer-Build-Transfer, to achieve a win-win situation for all parties.

Further, the HPCT sector's carbon emission pathways for 2020–2050 under 10 different policy scenarios are discussed. The carbon emissions in the HPCT sector are expected to peak in 2035 at around 119.6 % of the 2020 level if the targets of existing policies are met as expected. By 2050, it is expected to reduce carbon emissions by 56.66 % compared to 2020. With the single CER policy, the HPCT sector will achieve carbon peaking in 2030–2035. HESS is the single CER policy with the most significant carbon peak reduction, with a 9.66 % cut. ETV is the single CER policy with the earliest time to reach the carbon peak, advancing to 2030. This provides different options for the government to pursue peak time and peak reduction in the HPCT sector. However, a single CER policy is insufficient to achieve carbon neutrality in the HPCT sector by 2050. Under scenarios with multiple CER policies working together, the carbon peaking time will be expected to be advanced to 2030. Peak carbon-cutting benefits will be further increased to 10.4 %–18.66 %, and the 2050 CER benefits will reach 26.61 %–49.01 %. Among them, by adopting an aggressive combination CER policy of ETV + HESS or ETV + HESS+TDC, the HPCT sector's carbon emissions are expected to drop to less than 10 % in 2050 compared to 2020, basically achieving carbon neutrality. It requires the collaborative efforts of multiple sectors, including governments, the transportation sector, the energy sector, car manufacturers, and social investors, to deeply promote CER policies from multiple sources.

This study focuses on the 2020–2050 decarbonization pathway in the HPCT sector. The decarbonization pathway for lorries also needs attention. However, the decarbonization transition of lorries has not yet been given a clear development direction, with various new energy modes, including hydrogen, natural gas, battery swapping, and charging. In future studies, careful consideration of the green transition of passenger cars and lorries will hopefully lead to decarbonization in the road transport sector.

Appendix A. Abbreviation

Appendix B. Cost-benefit Model

B.1. Cost model

The cost of the HPSN project includes two parts: the initial investment cost and the operation and maintenance cost. Taking into account the time sequence influence, the total cost in ka , C^k is calculated as

$$C^k = C_{\text{init}}^k + C_{\text{O&M}}^k \quad (\text{A.1})$$

where C_{init}^k and $C_{\text{O&M}}^k$ are the initial investment cost and the operation and maintenance cost in ka .

(1) Initial investment cost in ka , C_{init}^k

The initial investment cost depends on the HPSN construction/expansion scale in ka . It includes equipment purchase cost, distribution facility cost, and land cost.

$$C_{\text{init}}^k = C_{\text{eq}}^k + C_{\text{dis}}^k + C_{\text{land}}^k \quad (\text{A.2})$$

(a) The equipment purchase cost in ka , C_{eq}^k

Funding information

Fundamental Research Funds for the Central Universities: 2023YJS151, General Program of National Natural Science Foundation of China: 52172312, National Key Research and Development Program of China: No. 2023YFB4302703, Singapore Ministry of Education Academic Research Fund (AcRF) Tier 1 project RT22/22.

CRediT authorship contribution statement

En-jian Yao: Resources, Funding acquisition, Data curation, Conceptualization. **Tian-yu Zhang:** Writing, Data curation, Results analysis, Conceptualization. **David Z.W. Wang:** Writing – review & editing, Project administration, Conceptualization. **Jun-yi Zhang:** Writing – review & editing, Supervision, Project administration.

Declaration of competing interest

The authors declare that they have no known competing financial interests or personal relationships that could have appeared to influence the work reported in this paper.

Data availability

The data that has been used is confidential.

Acknowledgements

No conflict of interest exists in the submission of this manuscript. I would like to declare on behalf of my co-authors that the work described is original unpublished work. This research was supported by Fundamental Research Funds for the Central Universities: 2023YJS151, General Program of National Natural Science Foundation of China: 52172312, National Key Research and Development Program of China: No. 2023YFB4302703, Singapore Ministry of Education Academic Research Fund (AcRF) Tier 1 project RT22/22.

The equipment of HPSN mainly includes fast chargers, WT generators, PV generators and ESs.

$$C_{\text{eq}}^k = \sum_{i \in I} \left(P_{\text{charger},i}^k \cdot N_{\text{charger},i}^k + P_{\text{WT},i}^k \cdot N_{\text{WT},i}^k + P_{\text{PV},i}^k \cdot N_{\text{PV},i}^k + P_{\text{ES},i}^k \cdot N_{\text{ES},i}^k \right) \quad (\text{A.3})$$

where P_{charger}^k is the unit price of charger in ka. P_{WT}^k , P_{PV}^k , and P_{ES}^k are the unit rated capacity price of WTs, Pvs and ESs in ka. $N_{\text{charger},i}^k$, $N_{\text{WT},i}^k$, $N_{\text{PV},i}^k$, and $N_{\text{ES},i}^k$ represent the constructed/expanded number of related equipment in ka.

(b) The distribution facility cost in ka, C_{dis}^k

The cost of the distribution facility related to the HPSN's capacity, such as transformers, switches, etc., also needs to be considered.

$$C_{\text{dis}}^k = \sum_{i \in I} P_{\text{dis}} \cdot \frac{N_{\text{charger},i}^k \cdot \nu_{\text{ch}} \cdot \delta_{\text{ch}}}{L_{\max} \cdot \alpha_{\text{cs}} \cdot \eta_{\text{ch}} \cdot \cos\phi_{\text{ch}}} \quad (\text{A.4})$$

where P_{dis} is the unit price of power distribution facility per unit capacity. ν_{ch} is the simultaneous charging rate. δ_{ch} is the rated output power of charger. L_{\max} is the maximum daily load rate of charging station. α_{cs} is the ratio of charging load to total load. η_{ch} and $\cos\phi_{\text{ch}}$ are charger's working efficiency, and power factor.

(c) The land cost in ka, C_{land}^k

$$C_{\text{land}}^k = \sum_{i \in I} P_{\text{land},i} \cdot y_i^k \quad (\text{A.5})$$

where $P_{\text{land},i}$ is the unit land price in area i . y_i^k is the binary variable indicating whether a station is built ($y_i^r = 1$) or not ($y_i^r = 0$) in candidate station i in the r th stage.

(2) Operation and maintenance cost in ka, $C_{\text{O&M}}^k$

The operation and maintenance costs are composed of electricity purchase costs, maintenance costs, labor charges, and equipment replacement costs.

$$C_{\text{O&M}}^k = C_{\text{buy}}^k + C_{\text{ma}}^k + C_{\text{lab}}^k + C_{\text{re}}^k \quad (\text{A.6})$$

(a) The power purchased cost from the grid in ka, C_{buy}^k

In HPSN's daily operation, the main cost is the power purchased cost from the grid, which is calculated as

$$C_{\text{buy}}^k = \sum_{i \in I} \sum_{t \in T} P_{\text{buy}} \cdot p_i^{t,k} \cdot N_{\text{year}} \quad (\text{A.7})$$

where P_{buy} is the power sale price of the grid. $p_i^{t,k}$ is the station i 's power demand at t moment in ka. N_{year} is the annual operation days of HPSN, there is 365d in one year.

(b) The maintenance cost in ka, C_{ma}^k

For equipment's ordinary repairment and overhaul during operation, the annual maintenance cost is as

$$C_{\text{ma}}^k = \sum_{k_1=0}^k C_{\text{init}}^{k_1} \cdot (\gamma_{\text{ma,c}} + \gamma_{\text{ma,a}}) \quad (\text{A.8})$$

where $\gamma_{\text{ma,c}}$ and $\gamma_{\text{ma,a}}$ are the annual common/accident maintenance coefficient.

(c) The labor wages in ka, C_{lab}^k

$$C_{\text{lab}}^k = P_{\text{lab}} \cdot N_{\text{lab}} \quad (\text{A.9})$$

where P_{lab} is the average level of local annual wages. N_{lab} is the number of labors required for the daily operation of a single charging station.

(d) The equipment replacement cost in ka, C_{up}^k

In order to guarantee the original HPSN service capacity, it is necessary to replace the expired equipment, including the charger, WT, PV, and ES.

$$C_{\text{re}}^k = C_{\text{re,charger}}^k + C_{\text{re,WT}}^k + C_{\text{re,PV}}^k + C_{\text{re,ES}}^k \quad (\text{A.10})$$

The equipment replacement cost is related to the equipment life, quantity, and use time. Taking the charger as an example, the charger replacement cost in ka is calculated

$$C_{\text{re,charger}}^k = \sum_{k_1=0}^k \sum_{i \in I} P_{\text{charger}} \cdot N_{\text{charger},i}^{k_1} \quad (\text{A.11})$$

$$\tau_{\text{charger}}^{k_1,k} = \begin{cases} 1, & (k - k_1) \% l_{\text{charger}} == 0 \\ 0 & \end{cases} \quad (\text{A.12})$$

where $\tau_{\text{charger}}^{k_1,k}$ is the binary variable indicating whether the charger building in k_1a is expired ($\tau_{\text{charger}}^{k_1,k} = 1$) or not ($\tau_{\text{charger}}^{k_1,k} = 0$) in ka . l_{charger} is the charger's life.

B.2. Benefit model

There are three main resources of HPSN's income: electricity sales income, construction subsidy, and end-of-life equipment salvage value.

$$I^k = I_{\text{sale}}^k + I_{\text{carbon}}^k + I_{\text{sub}}^k + I_{\text{sal}}^k \quad (\text{A.13})$$

(1) The power sales income in ka , I_{sale}^k

Selling power is the main income resource.

$$I_{\text{sale}}^k = \sum_{i \in I} \sum_{t \in T} (P_{\text{buy}} + P_{\text{ser}}) \cdot p_i^{t,k} \cdot N_{\text{year}} \quad (\text{A.14})$$

where P_{ser} is the unit charging service fee.

(2) The construction subsidy in ka , I_{sub}^k

Currently, construction subsidy is the main economic support for the government to encourage HPSN construction.

$$I_{\text{sub}}^k = C_{\text{init}}^k \cdot \gamma_{\text{sub}} \quad (\text{A.15})$$

where γ_{sub} is the government's subsidy coefficient for HPSN construction.

(3) The end-of-life equipment salvage value in ka , I_{sal}^k

$$I_{\text{sal}}^k = C_{\text{up}}^k \cdot \gamma_{\text{sal}} \quad (\text{A.16})$$

where γ_{sal} is the equipment's salvage value coefficient.

B.3. Parameter setting

The dynamic equipment price is set in [Table B1](#). And the other parameters are set in [Table B2](#).

Appendix C. Model linearization

The linearization process of Stage II model is illustrated as an example in Eq. (25). Eq. (25) is a complex nonlinear formula due to the presence of the nested nonlinear items, $\min(\cdot)$ and $\max(\cdot)$.

First, define two new variables $p_{i,t}^{1,k}$ and $p_{i,t}^{2,k}$ to to eliminate the nested $\min(\cdot)$ and $\max(\cdot)$. The original Eq. (25) can be decomposed into Eqs. (C-1)–(C-3).

$$p_{i,t}^{\text{R2E},k} = \min \left\{ p_{i,t}^{\text{W},k} + p_{i,t}^{\text{PV},k} - p_{i,t}^{\text{R2C},k}, p_{i,t}^{1,k} \right\} \quad \forall i \in \phi, t \in T_2, k \in K \quad (\text{C-1})$$

$$p_{i,t}^{1,k} = \max \left\{ 0, p_{i,t}^{2,k} \right\} \quad \forall i \in \phi, t \in T_2, k \in K \quad (\text{C-2})$$

$$p_{i,t}^{2,k} = \min \left\{ PE_i^k \cdot SOC_{\max} - PE_i^k \cdot SOC_{i,t}^k, E_i^k \right\} \quad \forall i \in \phi, t \in T_2, k \in K \quad (\text{C-3})$$

Further, the single nonlinear terms in Eqs. (C-1)–(C-3) are linearized to Eqs. (C-4)–(C-6) by introducing an infinity number M and six classes dummy variables $u_1^k, u_2^k, u_3^k, u_4^k, u_5^k, u_6^k$, respectively.

$$\left\{ \begin{array}{l} p_{i,t}^{W,k} + p_{i,t}^{PV,k} - p_{i,t}^{R2C,k} \geq p_{i,t}^{R2E,k}, p_{i,t}^{1,k} \geq p_{i,t}^{R2E,k} \\ p_{i,t}^{W,k} + p_{i,t}^{PV,k} - p_{i,t}^{R2C,k} \leq p_{i,t}^{R2E,k} - M(1 - u_1^k) \\ p_{i,t}^{1,k} \leq p_{i,t}^{R2E,k} - M(1 - u_2^k) \\ u_1^k + u_2^k \geq 1, u_1^k, u_2^k \in \{0, 1\} \\ \forall i \in \phi, t \in T_2, k \in K \end{array} \right. \quad (C-4)$$

$$\left\{ \begin{array}{l} p_{i,t}^{2,k} \leq p_{i,t}^{1,k}, 0 \leq p_{i,t}^{1,k} \\ p_{i,t}^{2,k} \geq p_{i,t}^{1,k} - M(1 - u_3^k) \\ 0 \geq p_{i,t}^{1,k} - M(1 - u_4^k) \\ u_3^k + u_4^k \geq 1, u_3^k, u_4^k \in \{0, 1\} \\ \forall i \in \phi, t \in T_2, k \in K \end{array} \right. \quad (C-5)$$

$$\left\{ \begin{array}{l} PE_i^k \cdot SOC_{max} - PE_i^k \cdot SOC_{i,t}^k \geq p_{i,t}^{2,k}, E_i^k \geq p_{i,t}^{2,k} \\ PE_i^k \cdot SOC_{max} - PE_i^k \cdot SOC_{i,t}^k \leq p_{i,t}^{2,k} - M(1 - u_5^k) \\ E_i^k \leq p_{i,t}^{2,k} - M(1 - u_6^k) \\ u_5^k + u_6^k \geq 1, u_5^k, u_6^k \in \{0, 1\} \\ \forall i \in \phi, t \in T_2, k \in K \end{array} \right. \quad (C-6)$$

References

- [1] Statista. Carbon dioxide emissions from energy consumption in the transportation sector in the U.S. from 1975 to 2022. <https://www.statista.com/statistics/1118464/transportation-co2-emissions-in-the-us-energy-consumption/>; 2023.
- [2] WRI, World Resources Institute. 4 Solutions to Enhance the Credibility of China's Subnational Transport Carbon Emissions Inventories. <https://www.wri.org/technical-perspectives/4-solutions-enhance-credibility-chinas-subnational-transport-carbon>; 2023.
- [3] Xiong S, Yuan Y, Zhang C. Achievement of carbon peak goals in China's road transport—possibilities and pathways. *J Clean Prod* 2023;388:135894.
- [4] Bansal P, Kockelman KM, Singh A. Assessing public opinions of and interest in new vehicle technologies: an Austin perspective. *Transport Res Part C: Emerg Technol* 2016;67:1–14.
- [5] Jia L, Ma J, Ji L, et al. Scenarios, patterns and solutions of ground transportation and energy convergence in China. Science Press; 2021.
- [6] Uslu T, Kaya O. Location and capacity decisions for electric bus charging stations considering waiting times. *Transp Res Part D: Transp Environ* 2021;90:102645.
- [7] Yang W, Liu W, Chung CY, Wen F. Joint planning of EV fast charging stations and power distribution systems with balanced traffic flow assignment. *IEEE Trans Industr Inform* 2020;17(3):1795–809.
- [8] He SY, Kuo YH, Wu D. Incorporating institutional and spatial factors in the selection of the optimal locations of public electric vehicle charging facilities: a case study of Beijing, China. *Transport Res Part C: Emerg Technol* 2016;67:131–48.
- [9] Bao Z, Xie C. Optimal station locations for en-route charging of electric vehicles in congested intercity networks: a new problem formulation and exact and approximate partitioning algorithms. *Transport Res Part C: Emerg Technol* 2021; 133:103447.
- [10] Lin Y, Zhang K, Shen ZJM, Ye B, Miao L. Multistage large-scale charging station planning for electric buses considering transportation network and power grid. *Transport Res Part C: Emerg Technol* 2019;107:423–43.
- [11] Xie F, Lin Z. Integrated US nationwide corridor charging infrastructure planning for mass electrification of inter-city trips. *Appl Energy* 2021;298:117142.
- [12] Zhang TY, Yao EJ, Yang Y, Pan L, Li CP, Li B, et al. Deployment optimization of battery swapping stations accounting for taxis' dynamic energy demand. *Transp Res Part D: Transp Environ* 2023;116:103617.
- [13] Zhang Q, Chen W. Modeling China's interprovincial electricity transmission under low carbon transition. *Appl Energy* 2020;279:115571.
- [14] Wang Y, Wang R, Tanaka K, Ciais P, Puelas J, Balkanski Y, et al. Accelerating the energy transition towards photovoltaic and wind in China. *Nature* 2023;619 (7971):761–7.
- [15] Yu Y, Wang J, Chen Q, Urpelainen J, Ding Q, Liu S, et al. Decarbonization efforts hindered by China's slow progress on electricity market reforms. *Nat Sustain* 2023; 1–10.
- [16] Lu X, McElroy MB, Peng W, Liu S, Nielsen CP, Wang H. Challenges faced by China compared with the US in developing wind power. *Nat Energy* 2016;1(6):1–6.
- [17] Colmenar-Santos A, Muñoz-Gómez AM, Rosales-Asensio E, López-Rey A. Electric vehicle charging strategy to support renewable energy sources in Europe 2050 low-carbon scenario. *Energy* 2019;183:61–74.
- [18] Victoria M, Zhu K, Brown T, Andresen GB, Greiner M. Early decarbonisation of the European energy system pays off. *Nat Commun* 2020;11(1):1–9.
- [19] Arbabzadeh M, Sioshansi R, Johnson JX, Keoleian GA. The role of energy storage in deep decarbonization of electricity production. *Nat Commun* 2019;10(1):3413.
- [20] He G, Lin J, Sifuentes F, Liu X, Abhyankar N, Phadke A. Rapid cost decrease of renewables and storage accelerates the decarbonization of China's power system. *Nat Commun* 2020;11(1):2486.
- [21] Zhuo Z, Du E, Zhang N, Nielsen CP, Lu X, Xiao J, et al. Cost increase in the electricity supply to achieve carbon neutrality in China. *Nat Commun* 2022;13(1): 3172.
- [22] Bellocchi S, Klöckner K, Manno M, Noussan M, Vellini M. On the role of electric vehicles towards low-carbon energy systems: Italy and Germany in comparison. *Appl Energy* 2019;255:113848.
- [23] Wang M, Wang Y, Chen L, Yang Y, Li X. Carbon emission of energy consumption of the electric vehicle development scenario. *Environ Sci Pollut Res* 2021;28: 42401–13.
- [24] Yu Y, Xu H, Cheng J, Wan F, Ju L, Liu Q, et al. Which type of electric vehicle is worth promoting mostly in the context of carbon peaking and carbon neutrality? A case study for a metropolis in China. *Sci Total Environ* 2022;837:155626.
- [25] Zhang TY, Yang Y, Zhu YT, Yao EJ, Wu KQ. Deploying public charging stations for battery electric vehicles on the expressway network based on dynamic charging demand. *IEEE Trans Transp Electrific* 2022;8(2):2531–48.
- [26] Zhou G, Dong Q, Zhao Y, Wang H, Jian L, Jia Y. Bilevel optimization approach to fast charging station planning in electrified transportation networks. *Appl Energy* 2023;350:121718.
- [27] Yang Y, Zhang T, Zhu YTY, Yao EJ. Optimal deploying of charging systems on an expressway network considering the optimal construction time sequence and the charging demand. *J Tsinghua Univ (Sci Technol)* 2022;62(07). 1163–1177+1219. [in Chinese].
- [28] Li S, Huang Y, Mason SJ. A multi-period optimization model for the deployment of public electric vehicle charging stations on network. *Transport Res Part C: Emerg Technol* 2016;65:128–43.
- [29] Zhang A, Kang JE, Kwon C. Incorporating demand dynamics in multi-period capacitated fast-charging location planning for electric vehicles. *Transp Res B Methodol* 2017;103:5–29.
- [30] Liang Y, Zhang X. Battery swap pricing and charging strategy for electric taxis in China. *Energy* 2018;147:561–77.
- [31] Bi Z, De Kleine R, Keoleian GA. Integrated life-cycle assessment and life-cycle cost model for comparing plug-in versus wireless charging for an electric bus system. *J Ind Ecol* 2017;21(2):344–55.
- [32] Yang M, Zhang L, Zhao Z, Wang L. Comprehensive benefits analysis of electric vehicle charging station integrated photovoltaic and energy storage. *J Clean Prod* 2021;302:126967.
- [33] Zhang Z, Sun X, Ding N, Yang J. Life-cycle environmental assessment of charging infrastructure for electric vehicles in China. *J Clean Prod* 2019;227:932–41.
- [34] ANL (Argonne National Laboratory). China vehicle fleet model: estimation of vehicle stocks, usage, emissions, and energy use—model description, technical documentation, and user guide. Lemont, IL: Argonne National Laboratory; 2018.
- [35] Gilbert C. Global passenger Car penetration: Grid lock!. Legal & General Investment Management Limited; 2017.

- [36] WRI, World Resources Institute. Toward “Net Zero” emissions in the road transport sector in China. 2019.
- [37] IEA, International Energy Agency. Global EV Outlook 2019. 2019.
- [38] Pesch T, Allelein HJ, Müller D, Withaut D. High-performance charging for the electrification of highway traffic: optimal operation, infrastructure requirements and economic viability. *Appl Energy* 2020;280:115706.
- [39] National Development and Reform Commission. Plan for modern energy system during the 14th five-year period. https://www.ndrc.gov.cn/xxgk/zcfb/ghb/202203/20220322_1320016.html; 2022.
- [40] Zhang T-Y, Yao E-J, Yang Y, Yang H-M, Wang DZW. Multi-network coordinated charging infrastructure planning for the self-sufficient renewable power highway. *Comput Aided Civ Inf Eng* 2024;1–24. <https://doi.org/10.1111/mice.13196>.
- [41] Inner Mongolia Autonomous Region Energy Bureau. Inner Mongolia Autonomous Region “Fourteenth Five-Year Plan” about Renewable Energy Development Plan. http://www.als.gov.cn/art/2022/8/2/art_73_445548.html. [Accessed 23 May 2023].
- [42] Inner Mongolia Autonomous Region People’s Government. Inner Mongolia Autonomous Region “Fourteenth Five-Year Plan” about comprehensive transportation development plan. https://www.nmg.gov.cn/zwgl/zfxgk/zfxgkml/202110/20211019_1911901.html. [Accessed 23 May 2023].
- [43] China Energy Storage Network. A list of details of photovoltaic, wind power installed capacity and power generation capacity in each province in. Available at: <http://escn.com.cn/news/show-1176657.html>. [Accessed 23 May 2023].
- [44] Zhang A, Kang JE, Kwon C. Incorporating demand dynamics in multi-period capacitated fast-charging location planning for electric vehicles. *Transp Res B Methodol* 2017;103:5–29.